Original Article

Binary B_2O_3–Bi_2O_3 glasses: scrutinization of directly and indirectly ionizing radiations shielding abilities

Check for updates

G. Lakshminarayana [a,*], Ashok Kumar [b], H.O. Tekin [c], Shams A.M. Issa [d,e], M.S. Al-Buriahi [f], Dong-Eun Lee [g,**], Jonghun Yoon [h,***], Taejoon Park [i,****]

[a] Intelligent Construction Automation Center, Kyungpook National University, 80, Daehak-ro, Buk-gu, Daegu, 41566, Republic of Korea
[b] Department of Physics, University College, Benra, Dhuri, Punjab, India
[c] Medical Diagnostic Imaging Department, College of Health Sciences, University of Sharjah, Sharjah, 27272, United Arab Emirates
[d] Department of Physics, Faculty of Science, University of Tabuk, Tabuk, Saudi Arabia
[e] Physics Department, Faculty of Science, Al-Azhar University, Assiut, 71452, Egypt
[f] Department of Physics, Sakarya University, Sakarya, Turkey
[g] School of Architecture, Civil, Environment and Energy, Kyungpook National University, 1370, Sangyeok-dong, Buk-gu, DaeGu, 702-701, Republic of Korea
[h] Department of Mechanical Engineering, Hanyang University, 55 Hanyangdaehak-ro, Ansan, Gyeonggi-do, 15588, Republic of Korea
[i] Department of Robotics Engineering, Hanyang University, 55 Hanyangdaehak-ro, Ansan, Gyeonggi-do, 15588, Republic of Korea

ARTICLE INFO

ABSTRACT

For five B_2O_3–Bi_2O_3 glasses, detailedly, γ, neutron, & proton, alpha, and electron (charged particles) shielding efficacies were assessed in this work. The crucial photon attenuating (interaction probabilities) parameter i.e., mass attenuation coefficient (μ/ρ) was calculated by Phy-X/PSD software and procured μ/ρ results have been verified through MCNPX, Geant4, & FLUKA codes μ/ρ findings from which a quality unanimity among them was noticed over an energy range of 15 KeV–15 MeV. Following μ/ρ & linear attenuation coefficient (μ) outcomes, Z_{eff}, N_{eff}, HVL, TVL, and MFP have been reckoned and found that all μ/ρ, Z_{eff}, N_{eff}, HVL, TVL, & MFP highly rest on glass chemical contents & photon energy. Z_{eq} and by applying geometric progression (G–P) fitting parameters (a, b, c, d, & X_k coefficients) EBFs & EABFs were appraised at ten specific penetration depths up to 40 mfp, at energy range of 0.015–15 MeV. The inferred RPE quantities confirmed all chosen glasses quintessential absorption competence for lower energy γ-rays. Utilizing SRIM code the mass stopping powers (MSPs) & projected ranges (PRs) for protons ((Ψ_P)&(Φ_P)) and alpha particles

* Corresponding author.
** Corresponding author.
*** Corresponding author.
**** Corresponding author.
E-mail addresses: gandham@knu.ac.kr (G. Lakshminarayana), dolee@knu.ac.kr (D.-E. Lee), yooncsmd@gmail.com (J. Yoon), taejoon@hanyang.ac.kr (T. Park).

$(\Psi_A)\&(\Phi_A)$, and with the help of ESTAR database, electron MSP (Ψ_E) & continuous slowing down approximation (CSDA) ranges for electrons have been approximated at 0.015 –15 MeV KE. The fast neutron removal cross-sections (Σ_R) were estimated and obtained Σ_R was diversified at 0.10978–0.12144 cm^{-1} range relying on Bi_2O_3 inclusion in glasses. Based on all acquired outputs, 57.5B_2O_3-42.5Bi_2O_3 (mol%) glass possesses superior attenuation capacity for γ-rays and fast neutrons as well as charged particles.

1.   Introduction

Despite the increasing demand for renewable energy resources like hydropower, solar energy, wind energy, and geothermal energy utilization, still, coal, oil, gas, and nuclear energy as non-renewable energy resources play a major role in energy supply globally. Further, being a clean energy origin with no pollution, minimal fuel costs, reuse option of recycled fuel, and reliability, nuclear energy for a few decades contributing considerably to the electricity generation. For instance, by the end of 2019, worldwide 450 nuclear power plants are actively functioning producing 10% of the world's electricity [1]. Both ^{235}U and ^{239}Pu radioactive sources are widely used nuclear fuels for power creation in nuclear reactors. However, there are some disadvantages associated with nuclear energy, mainly, dangers of accidents, exposure to ionizing radiations (α & β particles, X-rays, γ-rays, and neutrons), and nuclear waste creation. Besides, different radiopharmaceuticals (e.g., ^{99m}Tc, ^{111}In, ^{18}F, and ^{125}I, etc.) that are produced in nuclear reactors are employed in the nuclear medicine field together with imaging techniques to diagnose or treat various diseases [2]. So, for the protection of workers at nuclear power plants & medical staff and patients at where medicinal radiocompounds are used, from the deleterious effects of leaked or scattered and direct radiation exposure that emerge from the radioisotopes the installation of a rightful radiation shielding medium is obligatory. Moreover, to avoid radiation leakage from radioactive waste packages and to safeguard sensitive electronic equipment and astronauts in spacecraft during space missions from high energy radiations requires effective shielding composites [3,4]. Here, the desirable shielding (for γ & neutron) medium must contain both low-Z & high-Z elements in it with fewer irradiation effects on mechanical strengths over time, as alone low-Z compounds show poor photon attenuation capacity.

Classically, concrete (ordinary or heavyweight – holds aggregates like magnetite or barites) is being employed at nuclear power plants and radiotherapy facilities for nuclear radiation shielding as it mainly contains heavy nuclei to absorb γ-rays and H_2O (thus, H atoms) content to attenuate neutrons [5]. Though concrete is widely available, non-toxic, cheap, shows versatility for required any construction design, and needs less maintenance, it has some constraints such as opacity, immovability, cracks formation owing to free and bound H_2O loss by radiation heat, causing radiation leakage over prolonged use, and reduction in mechanical features under high neutron flux [6]. Apart from concretes, lead (Pb) or Pb found materials (glasses or bricks) are also extensively utilized in the past for shielding purposes at nuclear medical centers & nuclear reactors as Pb (Z = 82 & density (ρ) = 11.34 g/cm^3) possesses commendable X-ray and γ-ray attenuation ability. However, unlike concrete, Pb is costly, hard-to-utilize, toxic, and has inferior chemical durability. Particularly, because of Pb's toxicity effects on human health and environment, more recently, it is barely in use as a radiation shield at nuclear medicine centers [7]. From this perspective, numerous research groups have been, in recent years, thoroughly focussed on developing various kinds of Pb-free glasses, for example, Refs [8–11], which could be applied for radiation shielding, as principally glasses have low production costs relying on chemical constituents and are optically transparent. Also, glasses can be produced in large-scale using facile fabrication techniques (i.e., melt-quench or sol–gel approach) with high 'ρ', good mechanical & thermal strengths, and they are easily recyclable. Vitally, for a Pb-free glass to be used as a viable radiation shield, it is advisable to choose B_2O_3 or SiO_2-based glasses rather than TeO_2 or GeO_2 containing glasses without much compromising on glass 'ρ' as the former compounds are much cheaper than the latter ones.

It is widely known that B_2O_3 as a classic oxide glass former form glasses at lower melting points than SiO_2 glasses and are cost-effective than GeO_2 and TeO_2 glasses for large scale manufacturing, show fine optical transparency, good mechanical strength, and thermal stability. B_2O_3, as a glass component, considerably drops the SiO_2 glass melting temperatures, and it is a required component of nuclear waste glasses for high-level radioactive waste immobilization [12]. In 'B' (Z = 5) containing SiO_2 or other oxide glasses & melts, both trigonal ^{3}B & tetrahedral ^{4}B species of 'B' coevolve, though pure B_2O_3 glass contains only $[BO_{3/2}]$ structural units [13]. However, B_2O_3-rich glasses exhibit poor chemical durability with quick hydrolysis of $B^{[3,4]}$–O–$B^{[3,4]}$ bonds in the presence of H_2O and own relatively larger phonon energy (~1300–1500 cm^{-1}) than TeO_2 or GeO_2-based glasses [14]. Here, to improve chemical durability and to reduce phonon energy for practical photonic & optoelectronic applications heavy metal oxides (HMOs) like Bi_2O_3 (Bi (Z = 83)) can be included in an appropriate amount to B_2O_3-based glass compositions wherein Bi_2O_3 (Bi–O bond strength ~ 81.9 kcal/mol) acts as both network former & glass modifier, forming $[BiO_3]$ pyramidal & $[BiO_6]$ octahedral units, accordingly [15]. Bi_2O_3 also causes a high 'ρ' & refractive index, enhanced transparency over infrared (IR) region, and excellent nonlinear optical features in the glasses [16].

To utilize distinct substances, say, glasses as γ-ray absorbers, for them, meticulously evaluating the mass attenuation coefficient (μ/ρ) is essential either by proper experimental setup or using appropriate simulation processes (*e.g.*, FLUKA, MNCPX, Geant4, SRIM, Penelope, MCNP5, PHITS, etc.) and/or suitable theoretical approaches (*e.g.*, XMuDat, XCOM or WinXCOM, MicroShield®, BXCOM, Phy-X/PSD, etc.). Also, exploring 'μ', Z_{eff}, N_{eff}, HVL, TVL, MFP, RPE, Z_{eq}, EBF & EABF is vital for γ-ray attenuators. Next, estimations of mass stopping powers (MSPs) & projected ranges (PRs) for both protons (p) ((Ψ_P)&(Φ_P)) and alpha (α) particles (Ψ_A)&(Φ_A), electron (e^-) MSP (Ψ_E) & continuous slowing down approximation (CSDA) ranges for electrons, macroscopic effective removal cross-section for fast neutrons ($\sum_R$), and neutron total cross-section (σ_T) for thermal, slow, and intermediate energy neutrons are desirable to employ them for other directly & indirectly ionizing radiations shielding purpose in addition to γ-rays [17–20]. Concerning γ-rays (photons) as they possess no charge, interact differently than 'p', α & β particles and there happens three principal interactions (probabilistic, occasional manner) of photons with matter i.e., (a) Photoelectric absorption (PEA) (b) Compton scattering (CS) (incoherent scattering) and (c) pair production (PP) relying on incident photon energy and medium's ρ, Z_{eff} & N_{eff} whereas p, α & β particles interact with the medium in a certain, continuous nature. Moreover, Rayleigh scattering (RS) (coherent scattering), Thomson scattering (coherent/elastic scattering), and photonuclear reactions are the other insignificantly considered photon−matter interactions and specifically RS (causes no photon energy loss) phenomenon occur at the lowest γ-ray energies that too can be observed in narrow-beam geometry only.

Considering Pb-free glasses, more recently, Kurtulus & Kavas for SiO_2−Al_2O_3−Na_2O−MgO−CaO−SrO glass system [21], Olarinoye et al. [22] for $40TeO_2$-(60-x)V_2O_5-xMoO_3 (20 ≤ xMoO_3 ≤ 60 mol%) glasses, for $(25ZnO.75TeO_2)_{100-x}$ $(Ta_2O_5)_x$ (x = 0, 1, 2, 3 mol%) glasses by Kavaz et al. [23], for (60-x)B_2O_3+20Na_2O+20BaO + xHgO (x = 0, 2.5, 5, 7.5, 10, 12.5, 15 wt %) glasses by Abouhaswa & Kavaz [24], Al-Buriahi et al. [25] for (100−x)TeO_2+xZnO+4NiO (x = 9.6, 19.2, 28.8, 38.4 mol%) glasses, Akyildirim et al. [26] for (75-x)SiO_2−15Na_2O−10CaO-xZrO_2 (x = 0, 1, 3, 5, 7 mol%) glasses, for xBi_2O_3.10Li_2O.0.3CeO_2.9.7MoO_3(80-x)B_2O_3 (x = 0, 15, 30, 45, 60 wt%) glasses by Kaur et al. [27], Rammah et al. [28] for TeO_2−B_2O_3−Bi_2O_3−TiO_2 glass system, and for Bi_2O_3−Li_2O−MnO_2−B_2O_3 glass system by Kaur et al. [29] relevant nuclear radiation shielding features have been reported.

Being primary purpose of the current study is to examine the suitability of cheaper B_2O_3−Bi_2O_3 glass system as a potential nuclear radiation shield, we scrutinized, employing Phy-X/PSD program within the photon energy range of 15 KeV–15 MeV, μ, μ/ρ, Z_{eff}, N_{eff}, HVL, TVL, MFP, RPE, Z_{eq}, EBFs, and EABFs – for γ-ray shielding, Ψ_P, Φ_P, Ψ_A, Φ_A, Ψ_E, and CSDA ranges – for proton, α-, and e^- radiation attenuation by applying SRIM code (for proton & α-) and ESTAR database (for 'e^-') within 0.015 KeV–15 MeV kinetic energy (KE) range, and Σ_R – for fast neutrons attenuation using Phy-X/PSD. Likewise, μ/ρ quantities are also simulated utilizing MCNPX (v.2.6.0), Geant4, and FLUKA codes. The estimated lowest HVL & MFP are compared with respective distinct shielding materials

values. Up to 40 mfp PDs (penetration depths), through the G−P fitting formulae, both EBFs and EABFs are reckoned.

2. Materials and methods

For chosen all five binary B_2O_3−Bi_2O_3 glasses, the determined 'ρ' values were acquired from Ref. [30]. The considered five bismuth borate glasses, for simplicity, are indicated as 'B1', 'B2', 'B3', 'B4', and 'B5', accordingly. Related glass chemical compositions (in mol%) and associated computed elemental compositions (in wt%) along with the sample's 'ρ' selected in this work are given in Table 1. Utilizing B_2O_3 (99.98%) & Bi_2O_3 (99.99%) chemical powders in an accurate ratio, at 1273 K over 24 h heating in capped platinum (Pt) crucibles, after, casting into PtAu95/5 crucibles at 1273 K and then cooling (at 1 K/min rate) to ambient temperature (by cooling the glass melt in a regulated manner), all B1−B5 samples were synthesized [30]. At 290.7 K, through the hydrostatic weighing method, using H_2O as immersion fluid, all glasses 'ρ' was ascertained [30]. Following Table 1 data, one can observe that from B1→B5 glass, 'ρ' raises inevitably because of bigger molecular weight (M.W.) & 'ρ' of inserted Bi_2O_3 (465.96 g/mol & 8.9 g/cm^3) instead of lesser M.W. & 'ρ' B_2O_3 (69.63 g/mol & 2.46 g/cm^3). Here, average M.W. of B1, B2, B3, B4, and B5 glasses are 148.888 g/mol, 168.705 g/mol, 188.522 g/mol, 208.339 g/mol, and 238.0645 g/mol, respectively, and calculated molar volume (V_m) is 34.609 cm^3/mol, 34.620 cm^3/mol, 35.048 cm^3/mol, 35.711 cm^3/mol, 36.961 cm^3/mol, correspondingly, for the same samples. Thus, while 'ρ' increases 'V_m' also enhanced for all B1−B5 glasses. Usually, compared to 'ρ', 'V_m' is highly susceptible to structural variations (atoms spatial distribution) among samples as 'V_m' regulates for various glass chemical constituents' atomic weights.

Statements with related formulae or expressions for μ, μ/ρ, Z_{eff}, N_{eff}, HVL, TVL, MFP, RPE, Z_{eq}, and geometric progression (G−P) fitting process for EBFs and EABFs prediction were reported earlier in numerous publications [8,9,11,17–20,23,26–28,31], including about Σ_R [9,17,18,20] and they are not rephrased here. When protons and α-particles or charged particles pass through a shield, by interacting with atoms they gradually lose KE and here, per a unit path length, the KE decrement is expressed as 'linear stopping power (LSP) (S(E) = dE/dx)' and can be deduced by the following relation [32]:

Table 1 − Chemical composition (mol%) and elements (wt %) present in the selected binary B_2O_3−Bi_2O_3 glasses, including their density [30].

Glass code	Glass composition (mol%)		Elemental composition (wt%)			Density (g/cm^3)
	B_2O_3	Bi_2O_3	B	Bi	O	
B1	80	20	11.6179	56.1448	32.2373	4.302
B2	75	25	9.6124	61.9371	28.4505	4.873
B3	70	30	8.0285	66.5117	25.4598	5.379
B4	65	35	6.7459	70.2160	23.0381	5.834
B5	57.5	42.5	5.2224	74.6161	20.1615	6.441

$$-\frac{dE}{dx} = \frac{4\pi N_A m_e c^2 r_e^2 \mathscr{Z}^2}{\beta^2} \rho \frac{Z}{A} \ln 4 \pi\varepsilon_o \frac{\gamma^2 m_e v^3}{\mathscr{Z} e^2 f} \qquad (1)$$

where $r_e = \frac{e^2}{4\pi\varepsilon_o m_e c^2}$ = electron radius, $\beta = \frac{v}{c}$, and. $N_e = Z\frac{N_A}{A}\rho$.

Then, mass stopping power (MSP) can be calculated by LSP/ρ. Further, following Eq. (1), for protons and α-particles, projected range (PR) in a substance could be estimated by the below expression [28]:

$$R = \int_0^R dx = \int_E^0 \frac{dx}{dE} dE = \int_0^E \frac{dE}{S(E)} \qquad (2)$$

where $S(E) = -\frac{dE}{dx}$, 'PR' predominantly reckons on the charge, KE, mass, and 'ρ' of the protons or α-particles (charged particles).

For electrons (charged particles), it can be approximated that they continuously and progressively degrade in KE during collisions with materials atoms. Here, the term CSDA (continuous slowing down approximation) range represents the integral of the SP reciprocal over KE from a terminal to an initial quantity as below [33]:

$$R_{CSDA} = \int_0^{(E_K)_0} \frac{dE}{S_{total}(E)} \qquad (3)$$

where R_{CSDA} = in a composite, charged particles CSDA diffusion distance, E_K = initial KE, and $S_{total}(E)$ = total MSP in line with E_K.

For all B1—B5 glasses, in this study $((\Psi_P)\&(\Phi_P))$ and $(\Psi_A)\&(\Phi_A)$ against KE are computed using SRIM (Stopping and Range of Ions in Matter) codes established by Ziegler et al. [34]. Moreover, the Ψ_E & CSDA range values versus KE are estimated with the help of the ESTAR database (https://physics.nist.gov/PhysRefData/Star/Text/ESTAR.html) [35]. For details about utilized Phy-X/PSD (Photon Shielding and Dosimetry) software readers' can check Ref. [36] and https://phy-x.net/PSD web page, as they are not described here. Employed both MCNPX (Monte Carlo N-Particle eXtended) [37] & Geant4 (for GEometry ANd Tracking) [38,39,40] simulation geometry (Figs. 1 and 2) processing specifics are the same as we supplied in our recent works [19,25,31,41] and are not repeated here. Next, Fig. 3 illustrates the simulation setup for exercised FLUKA (FLUktuirende KAskade) code (http://www.fluka.org/) and for particulars of this code (created conjunctly by Italian Institute for Nuclear Physics (INFN) & European Organization for Nuclear Research (CERN)) readers' can refer to Refs. [42,43].

3. Results and discussion

In this research, for all B1—B5 samples, the related photon attenuation qualities i.e., μ, μ/ρ, Z_{eff}, N_{eff}, HVL, TVL, MFP, Z_{eq}, EBF, EABF, and RPE, unless stated otherwise, are attained within 0.015—15 MeV energy range. Essentially, to consider any medium such as glass or alloy or polymer composite or concrete or ceramic, etc. as a potential γ-ray shield it must possess sufficiently higher 'ρ', larger μ, μ/ρ, Z_{eff}, Z_{eq}, & RPE, and lower HVL, TVL, MFP, EBFs, & EABFs. Vitally, at corresponding lower, intermediate, and higher photon energies, certain PEA, CS, and PP phenomenon plays an influential role in any

material. Here, relying on substance 'Z' and incident photon energy (E), PEA $\propto E^{-3.5}/Z^{4-5}$, CS $\propto E^{-1}/Z$, and PP $\propto \log E/Z^2$ [8–11,17–29,31]. So, with an increment in E, the odds of PEA reduce, and if the materials' Z enhances, the chances of the PEA increase. Incoherent CS scattering also decreases with E, but not as fast as the PEA. PP mechanism does not happen at E < 1.022 MeV and after this threshold is approached, it occurs probably as E improves.

Fig 4 exemplifies the 'μ' transitions, calculated using Phy-X/PSD, for all B1—B5 samples. Here, 'μ' exhibits an akin drift within examined 'E' range for all chosen glasses and Bi_2O_3 inclusion instead of B_2O_3 causes improvement in 'μ' from B1$\rightarrow$B5 glass as Bi (Z) = 83 > B (Z) = 5. Consequently, glass B5 (contained 'Bi' wt% = 74.6161 wt%, see Table 1) has the highest 'μ' in all investigated samples. 282.87 cm^{-1}, 352.7597 cm^{-1}, 417.5869 cm^{-1}, 477.6746 cm^{-1}, and 559.8516 cm^{-1}, for example, are the derived respective 'μ' values for B1, B2, B3, B4, and B5 samples at 15 KeV 'E'. Further, owing to PEA dominance from 15 KeV$\rightarrow$0.4 MeV 'E', 'μ' reduced sharply, though there occurs a quick rise in it at 0.1 MeV because of Bi element K-absorption edge (=90.53 KeV), for all B1—B5 glasses. In PEA, 'E' can be totally absorbed by an inner shell (e.g., K shell) electron. Next, beyond 0.4 MeV up to 6 MeV 'E' for B1 & B2 samples, and up to 5 MeV 'E' for B3, B4, & B5 glasses, due to CS process influence, 'μ' deviated or decreased minimally. CS phenomenon is commonly the very likely kind of interaction in materials. Afterward, above 6 MeV for B1 & B2 glasses and beyond 5 MeV for B3, B4, & B5 samples, up to 15 MeV 'E', on account of PP mechanism, 'μ' enhanced slightly. In the PP process, excessive 'E' >1.022 MeV turns as the KE for positrons & electrons. At 5 & 15 MeV 'E', for instance, for B5 glass, the calculated according 'μ' quantities are 0.251877 cm^{-1} & 0.304198 cm^{-1}.

Table 2 (i-iv) presents the pertinent μ/ρ outcomes computed by Phy-X/PSD software, MCNPX, Geant4, & FLUKA codes for all B1—B5 glasses and Fig. 5 (a-e) clarifies the achieved μ/ρ comparisons for these samples, accordingly. Here, produced by four distinct methods, at all chosen 'E', the acquired μ/ρ results are identified to be in tune among themselves. Usually, because of small disparities in the selected geometry and physical models for μ/ρ simulations in specific methods, fewer inequalities could possible in the outputs between computational and theoretical techniques. As an example, by Phy-X/PSD, and MCNPX, Geant4, & FLUKA codes at 0.015 MeV 'E', 86.92 cm^2/g, 84.3951 cm^2/g, 85.6117 cm^2/g, & 86.298 cm^2/g, correspondingly, are the deduced μ/ρ quantities for sample B5 while these obtained values for the same glass at 15 MeV 'E' with the mentioned same four methods are 0.0472 cm^2/g, 0.0475 cm^2/g, 0.0465 cm^2/g, & 0.0468 cm^2/g, consecutively. It is evident from Fig. 5 & Table 2 that as the 'E' increases, the μ/ρ values are reduced for all B1—B5 samples. Moreover, Bi_2O_3 insertion in place of B_2O_3, i.e., 'ρ' increment from 4.302 $\rightarrow$ 6.441 g/cm^3 has led to the μ/ρ enhancement from B1$\rightarrow$B5 glass, where all samples show an identical μ/ρ inclinations with improving 'E'. For instance, utilizing Geant4 code, at 15 KeV 'E', the simulated μ/ρ values are 64.8562 cm^2/g, 71.031 cm^2/g, 76.5746 cm^2/g, 80.332 cm^2/g, and 85.6117 cm^2/g, accordingly, for B1, B2, B3, B4, and B5 glasses. At the minimal 'E', μ/ρ quantities are high for all B1—B5 samples as the PEA commands this region where within 15 KeV–0.05 MeV 'E' – a
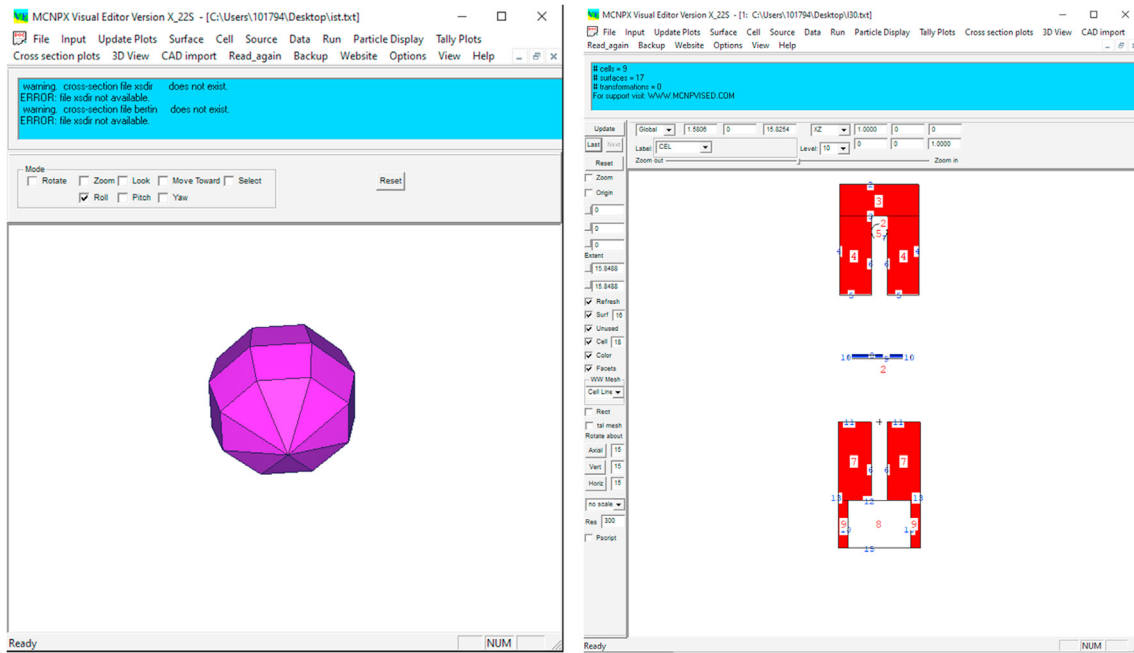
(a)

(b)
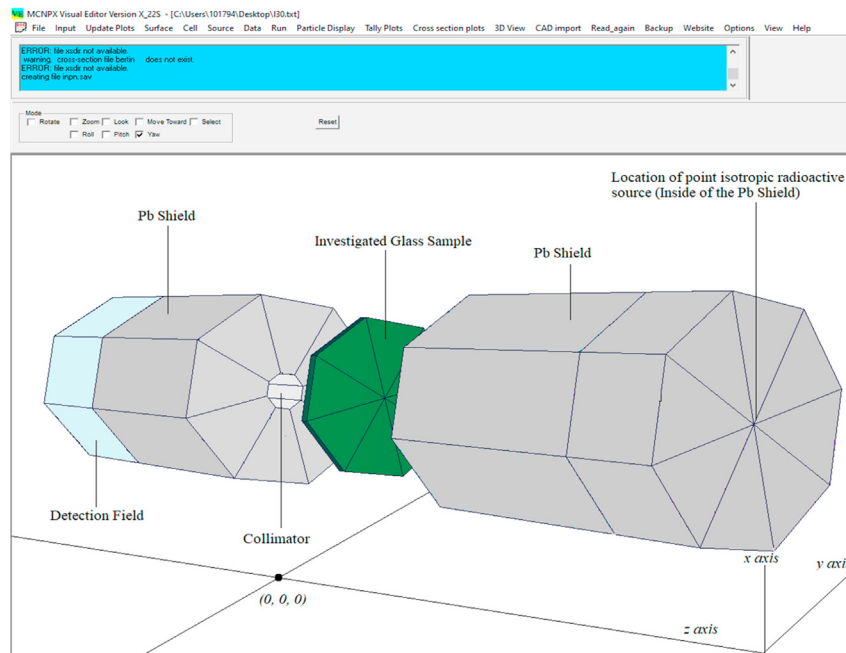
(c)

Fig. 1 – (a) Modeled point isotropic radioactive source obtained from MCNPX Visual Editor (b) 2-D view of simulation setup drawn from MCNPX Visual Editor (version X_22 S) and (c) 3-D view of employed MCNPX simulation setup (photon transmission setup) obtained from MCNPX Visual Editor.

quick decline & >0.05 → 0.3 MeV 'E' – a small reduction in μ/ρ has been noticed. For >0.3→(5−8) MeV 'E', fewer decrements or fluctuations are observed in μ/ρ as the CS phenomenon dominates in this region, and at (>5−8)→15 MeV 'E' range for all studied glasses μ/ρ marginally improved due to PP process

dominance in this range. In all μ/ρ patterns, the noticed small jump at 100 KeV energy close to the Bi: K-absorption edge can be related to PEA impact. Glass B5 possesses the highest μ/ρ for inspected 'E' range among all selected samples, evincing it as an optimum γ-ray shield.
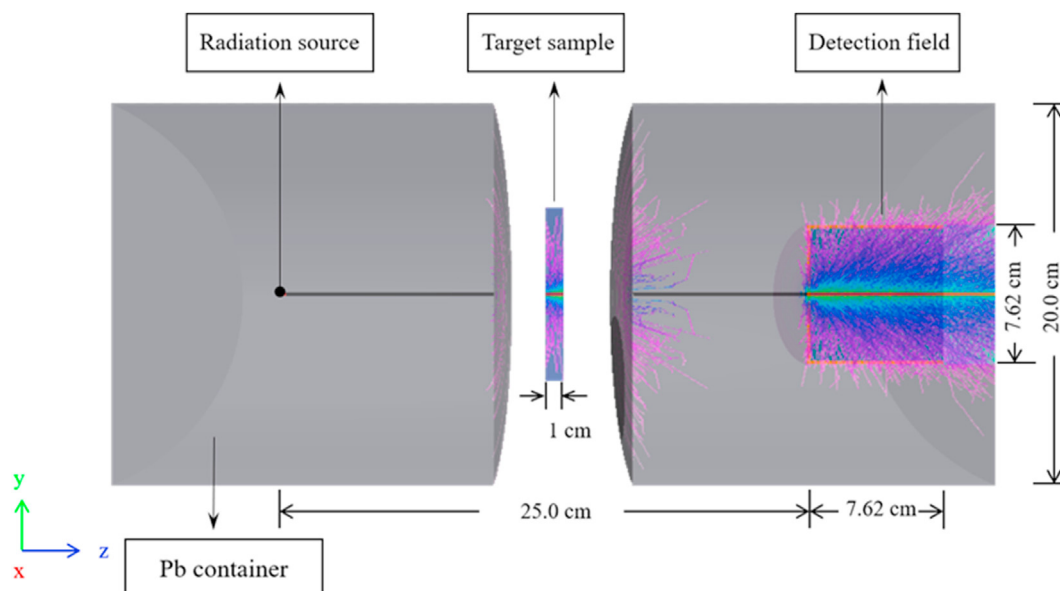
Fig. 2 — Sketch of simulation geometry used for Geant4 code (dimensions are in 'cm' units).
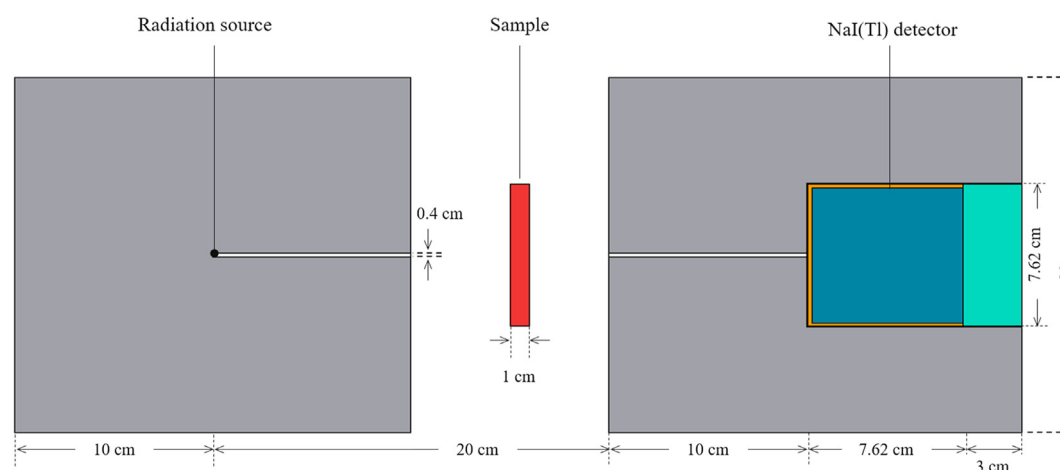

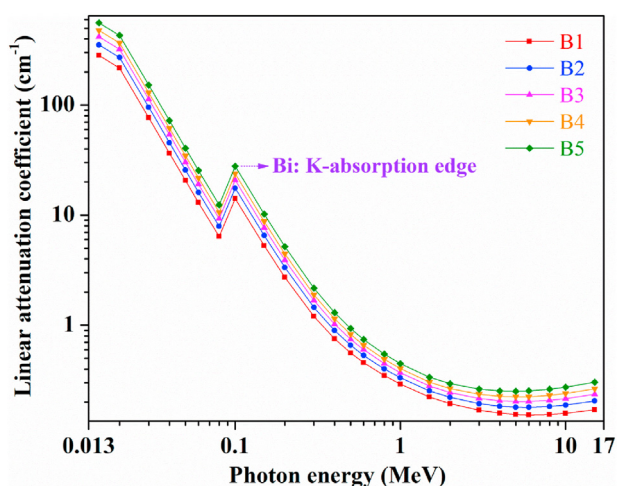**Fig. 3 — Sketch of simulation geometry utilized for FLUKA code (dimensions are in 'cm' units).**

Fig. 4 — Variation of linear attenuation coefficient (μ, cm^{-1}) with photon energy (MeV) for all B1—B5 glasses.

The determined Z_{eff} & N_{eff} variations within probed 'E' range are displayed in Figs. 6 and 7, correspondingly, for all B1—B5 samples. For any shield, both Z_{eff} & N_{eff} values play critical roles in radiation therapy for the estimation of absorbed dose & correct dose delivery required to the patients. Here, for all studied glasses, Z_{eff} & N_{eff} profiles reveal alike directions with 'E'. Following Figs. 6 and 7, one can identify that from B1→B5 glass, with continuous Bi_2O_3 addition in lieu of B_2O_3, Z_{eff} increases steadily whereas N_{eff} values follow an opposite movement to Z_{eff}, i.e., sample B5 possesses the largest Z_{eff} and the minimal N_{eff} quantities in all selected glasses. Generally, the greater the Z_{eff}, the higher the photons interaction with a medium, leading to less number of γ-rays or X-rays escape from it. For all B1—B5 samples, because of PEA, maximal quantities of Z_{eff} & N_{eff} are noticed in the lower 'E' range as 'Bi' (high-Z) present in all glasses. For instance, 75.61, 77.02, 77.99, 78.7, and 79.47 are the Z_{eff} quantities at 15 KeV 'E' for respective B1, B2, B3, B4, and B5 glasses while at the same 'E', for these samples, the calculated relevant N_{eff} values are

Table 2 – Mass attenuation coefficients (μ/ρ) of all B1–B5 glasses derived utilizing (i) Phy-X/PSD program (ii) MCNPX (v.2.6.0) (iii) Geant4 and (iv) FLUKA codes.

Energy (MeV)	B1	B2	B3	B4	B5
(i) Phy-X/PSD program					
0.015	65.753	72.391	77.633	81.878	86.92
0.02	50.570	55.716	59.781	63.072	66.981
0.03	17.840	19.647	21.074	22.23	23.603
0.04	8.499	9.3517	10.025	10.57	11.218
0.05	4.792	5.2659	5.6401	5.9432	6.3032
0.06	3.018	3.3106	3.5417	3.7289	3.9513
0.08	1.487	1.6238	1.7318	1.8192	1.9231
0.1	3.287	3.6111	3.8667	4.0737	4.3196
0.15	1.227	1.3404	1.4297	1.5019	1.5877
0.2	0.633	0.6861	0.7279	0.7617	0.8019
0.3	0.280	0.2978	0.3121	0.3237	0.3374
0.4	0.175	0.1838	0.1905	0.1959	0.2023
0.5	0.130	0.1351	0.1388	0.1418	0.1454
0.6	0.106	0.1092	0.1115	0.1133	0.1154
0.8	0.081	0.0824	0.0834	0.0842	0.0851
1	0.068	0.0685	0.0689	0.0693	0.0698
1.5	0.052	0.0521	0.0522	0.0523	0.0524
2	0.045	0.0455	0.0456	0.0458	0.0459
3	0.039	0.0399	0.0403	0.0406	0.0409
4	0.037	0.0378	0.0384	0.0388	0.0394
5	0.036	0.037	0.0378	0.0384	0.0391
6	0.036	0.0369	0.0378	0.0386	0.0394
8	0.036	0.0376	0.0388	0.0397	0.0408
10	0.037	0.0388	0.0402	0.0413	0.0426
15	0.040	0.0422	0.044	0.0455	0.0472
(ii) MCNPX (v.2.6.0) code					
0.015	63.9652	70.4585	75.4524	79.5126	84.3951
0.02	49.5126	54.3622	58.2654	61.3853	65.1956
0.03	17.2413	18.8156	20.1956	21.2426	22.6124
0.04	7.9626	8.7607	9.4120	9.9112	10.5239
0.05	4.4120	4.8512	5.1902	5.4682	5.8004
0.06	2.7398	3.0047	3.2106	3.3841	3.5812
0.08	1.3124	1.4178	1.5198	1.5974	1.6904
0.1	3.1653	3.4853	3.7226	3.9207	4.1571
0.15	1.1672	1.2836	1.3652	1.4284	1.5092
0.2	0.6012	0.6527	0.6884	0.7170	0.7541
0.3	0.2631	0.2791	0.2926	0.3029	0.3150
0.4	0.1662	0.1734	0.1791	0.1841	0.1891
0.5	0.1243	0.1293	0.1316	0.1338	0.1369
0.6	0.1019	0.1051	0.1071	0.1079	0.1101
0.8	0.0799	0.0796	0.0812	0.0810	0.0823
1	0.0674	0.0670	0.0672	0.0682	0.0684
1.5	0.0536	0.0521	0.0523	0.0517	0.0523
2	0.0451	0.0462	0.0462	0.0462	0.0456
3	0.0404	0.0401	0.0411	0.0414	0.0413
4	0.0381	0.0380	0.0391	0.0392	0.0395
5	0.0376	0.0373	0.0382	0.0390	0.0398
6	0.0361	0.0371	0.0386	0.0391	0.0403
8	0.0365	0.0377	0.0391	0.0401	0.0412
10	0.0372	0.0390	0.0412	0.0416	0.0430
15	0.0408	0.0431	0.0443	0.0459	0.0475
(iii) Geant4 code					
0.015	64.8562	71.0310	76.5746	80.3320	85.6117
0.02	49.9339	55.0380	58.7548	62.4240	65.9340
0.03	17.5625	19.3256	20.7288	21.8642	23.1739
0.04	8.3613	9.1913	9.9141	10.4596	10.9824
0.05	4.7503	5.2297	5.5567	5.9093	6.2491
0.06	2.9952	3.2904	3.5007	3.7010	3.8907
0.08	1.4679	1.6071	1.7147	1.8043	1.8896
0.1	3.2549	3.5677	3.8368	4.0517	4.2805
0.15	1.2129	1.3230	1.4161	1.4936	1.5632
0.2	0.6251	0.6761	0.7241	0.7536	0.7916
0.3	0.2759	0.2937	0.3086	0.3199	0.3325
0.4	0.1736	0.1812	0.1882	0.1935	0.2003
0.5	0.1288	0.1336	0.1379	0.1406	0.1442
0.6	0.1054	0.1080	0.1099	0.1123	0.1137
0.8	0.0807	0.0817	0.0823	0.0833	0.0844
1	0.0673	0.0676	0.0682	0.0684	0.0690
1.5	0.0515	0.0516	0.0515	0.0516	0.0519
2	0.0447	0.0451	0.0454	0.0454	0.0456
3	0.0391	0.0396	0.0400	0.0400	0.0404
4	0.0365	0.0373	0.0379	0.0382	0.0389
5	0.0357	0.0365	0.0373	0.0380	0.0386
6	0.0352	0.0365	0.0376	0.0381	0.0388
8	0.0359	0.0371	0.0385	0.0393	0.0402
10	0.0364	0.0383	0.0398	0.0409	0.0423
15	0.0393	0.0417	0.0434	0.0448	0.0465
(iv) FLUKA code					
0.015	65.3893	72.1961	77.1494	81.7293	86.2980
0.02	50.5000	55.6335	59.6379	62.4692	66.7426
0.03	17.7370	19.4593	21.0249	22.1798	23.3200
0.04	8.4384	9.2748	9.9676	10.4932	11.0738
0.05	4.7816	5.2444	5.6355	5.9238	6.2704
0.06	2.9933	3.3047	3.5241	3.7135	3.9320
0.08	1.4868	1.6205	1.7236	1.8183	1.9064
0.1	3.2704	3.5878	3.8373	4.0467	4.2841
0.15	1.2194	1.3323	1.4204	1.4944	1.5789
0.2	0.6312	0.6855	0.7269	0.7589	0.7968
0.3	0.2777	0.2973	0.3111	0.3210	0.3347
0.4	0.1737	0.1827	0.1895	0.1959	0.2018
0.5	0.1297	0.1340	0.1387	0.1415	0.1448
0.6	0.1062	0.1083	0.1110	0.1132	0.1150
0.8	0.0810	0.0821	0.0828	0.0837	0.0845
1	0.0678	0.0680	0.0684	0.0693	0.0695
1.5	0.0519	0.0518	0.0518	0.0523	0.0520
2	0.0451	0.0451	0.0452	0.0456	0.0458
3	0.0391	0.0396	0.0400	0.0402	0.0406
4	0.0369	0.0377	0.0381	0.0386	0.0391
5	0.0360	0.0369	0.0377	0.0383	0.0388
6	0.0355	0.0368	0.0377	0.0385	0.0393
8	0.0359	0.0372	0.0387	0.0397	0.0407
10	0.0368	0.0384	0.0400	0.0413	0.0424
15	0.0397	0.0420	0.0438	0.0453	0.0468

15.29×10^{23}, 13.75×10^{23}, 12.46×10^{23}, 11.37×10^{23}, and 10.05×10^{23} electrons/g. Both Z_{eff} & N_{eff} reduces significantly with raising 'E' up to 0.5 MeV with a sudden hike at 0.1 MeV (near Bi: K-absorption edge, by virtue of PEA). Later, owing to the CS process, at E > 0.5 → 1.5 MeV, for all chosen glasses, computed both Z_{eff} & N_{eff} fluctuates or declines negligibly. The lowest Z_{eff} & N_{eff} derived for B1, B2, B3, B4, and B5 samples at 1.5 MeV 'E' are (14.59, 16.49, 18.36, 20.21, and 22.95) & (2.951×10^{23}, 2.943×10^{23}, 2.932×10^{23}, 2.921×10^{23}, and 2.903×10^{23} electrons/g), accordingly. With further 'E' increment above 1.5 MeV up to 15 MeV, Z_{eff} & N_{eff} quantities exhibit a progressive rise due to PP phenomenon predominance in this region. Here, Fig. 6 results firmly endorse that for better photon attenuation potency of B_2O_3–Bi_2O_3 glasses, a greater content of Bi_2O_3 is essential in them. As sample B5 owns relatively bigger Z_{eff} in all tested glasses, it can be utilized as a superior shield regarding γ-rays. Further, N_{eff} deviates at 10.05×10^{23} (0.015 MeV 'E') – 5.237×10^{23} (15 MeV 'E') electrons/g range, for glass B5.

Fig. 8 (a), (b) and Fig. 9 illustrates the approximated changes of HVL, TVL, & MFP quantities with 'E', accordingly,
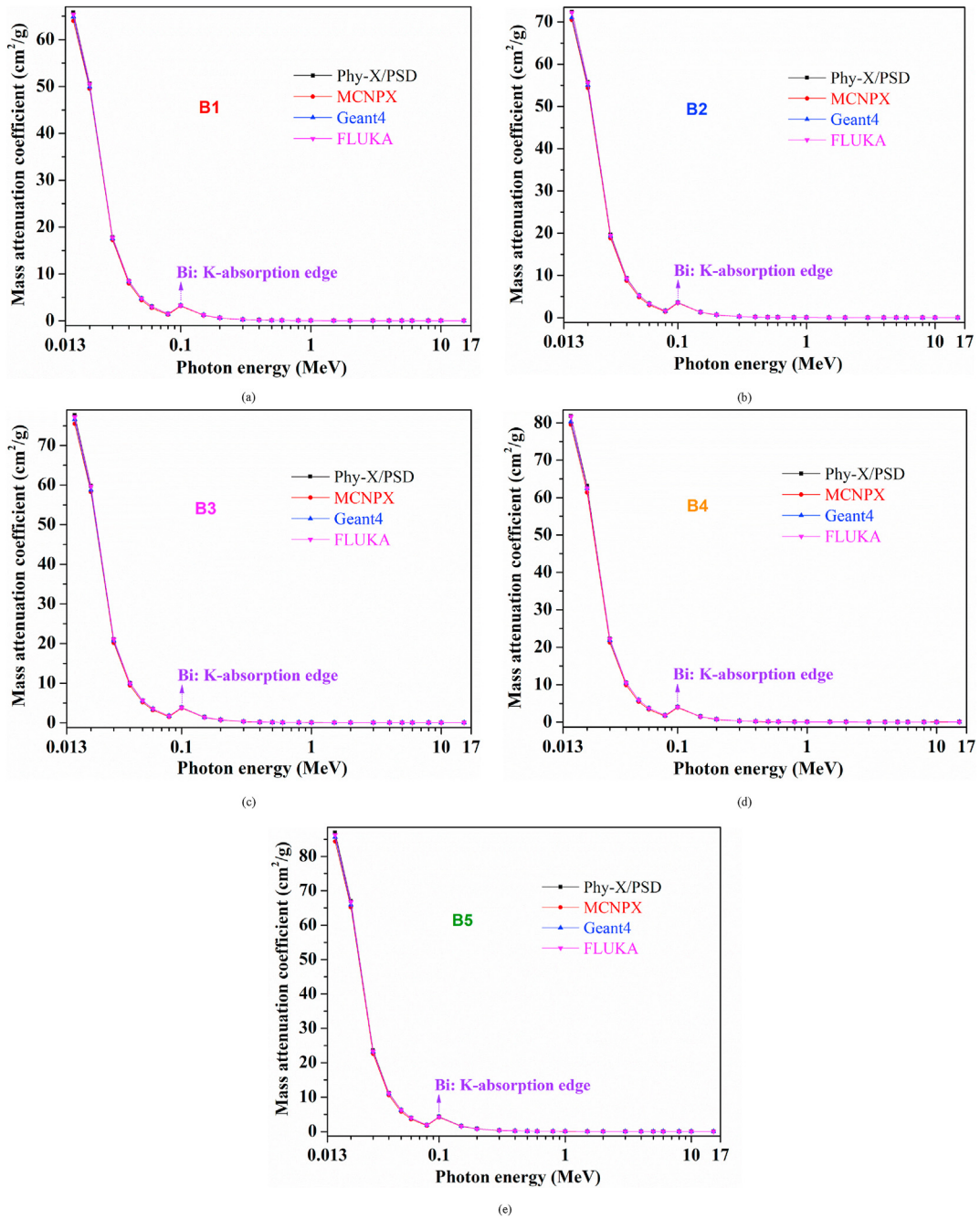
Fig. 5 — (a—e). Comparison of Phy-X/PSD program, MCNPX, Geant4, and FLUKA codes derived mass attenuation coefficients (cm^2/g) versus photon energy for all B1—B5 glasses.

for all B1—B5 samples whereas the corresponding inset plots visualize the enlarged 'E' range at 0.029—0.16 MeV. Here, calculated all HVL, TVL, & MFP values exhibit similar deviations within investigated 'E' range. From Figs. 8 and 9, one can notice that from 0.015 → 0.1 MeV 'E', related HVL, TVL, & MFP are minimal (i.e., a tiny part of 'cm'), indicating that a smaller thickness B1—B5 glasses are adequate to attenuate photons within this energy range. Then, with increasing 'E' beyond 100 KeV up to 6 MeV for samples B1 & B2, and up to 5 MeV for B3, B4, & B5 glasses all HVL, TVL, & MFP increase swiftly attaining the respective maximal values, specifying greater thickness obligation for samples to decrease incident

photons energy. For example, to reduce incoming 5 MeV 'E' γ-ray to 50% of its initial intensity about 2.752 cm thickness sample B5 is essential. Likewise, the derived MFP quantities at 6 MeV 'E' for B1 & B2 glasses and at 5 MeV 'E' for B3, B4, and B5 samples are 6.501 cm, 5.56 cm, 4.922 cm, 4.466 cm, and 3.97 cm, accordingly. Thereafter, at >6 MeV 'E' (for B1 & B2 samples), >5 MeV 'E' (for B3, B4, and B5 glasses) up to 15 MeV 'E', all the obtained HVL, TVL, & MFP showed a decreasing trend. For instance, 2.279 cm, 7.569 cm, & 3.287 cm are the deduced respective HVL, TVL, & MFP values at 15 MeV 'E' for glass B5. As briefed for Figs. 4—7 results, here also, with 'E', all the noticed HVL, TVL, & MFP alterations are
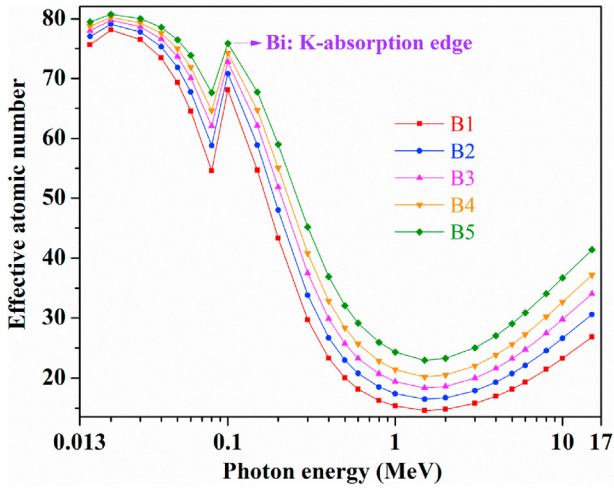
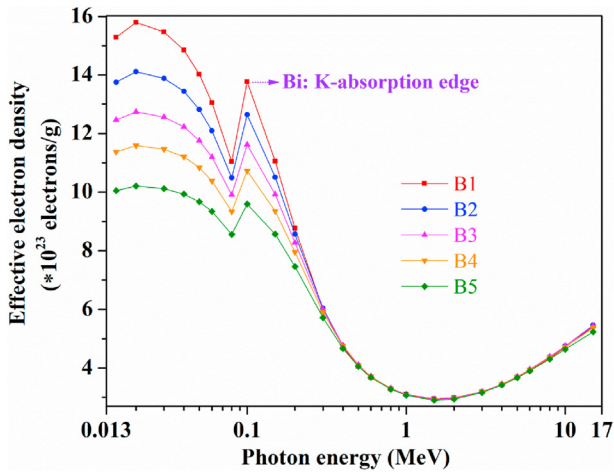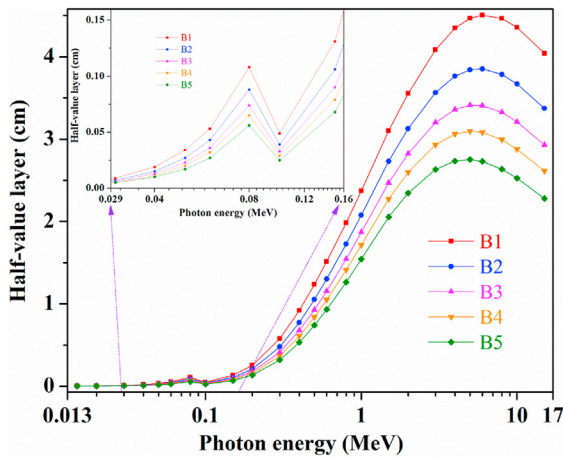**Fig. 6 – Variation of effective atomic number (Z_{eff}) with photon energy (MeV) for all B1–B5 glasses.**

Fig. 7 – Variation of effective electron density (N_{eff}) with photon energy (MeV) for all B1–B5 glasses.
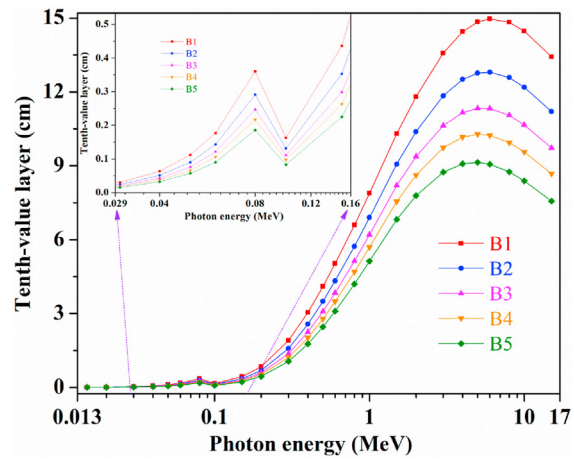
caused by PEA, CS, and PP actions preeminence at discrete ranges. Besides, seemingly, at all checked out energies, improving the Bi_2O_3 amount from 20 → 42.5 mol% from B1→B5 glass has led to a decline in HVL, TVL, & MFP (see Figs. 8 and 9). Here, relatively less thickness is enough for glass B5 than remaining glasses to shield photons as 'ρ' enhances from B1→B5 glass (see Table 1). As an example, 0.053 cm, 0.043 cm, 0.036 cm, 0.032 cm, and 0.027 cm, & 0.077 cm, 0.062 cm, 0.052 cm, 0.046 cm, and 0.039 cm are the computed corresponding HVL & MFP for B1, B2, B3, B4, and B5 samples at 60 KeV 'E' which is commonly utilized in computed tomography (CT).

Relevantly, sample B5 HVL & MFP are related with reported respective quantities of commercial shielding glasses (SCHOTT AG: RS 253, RS 253 G18, RS 323 G19, RS 360, and RS 520) [44], SS403, CN, CS516, IL600, and MN400 alloys [45], natural rubber, polyacrylonitrile, polyethylacrylate, polyethylene tetraphthalate, polyoxymethylene, and polyphenyl methacrylate polymers [46], OC, BMC, HSC, IC, ILC, SMC, and SSC [47], and lead (Pb), including calcium silicide ($CaSi_2$), magnesium silicide (Mg_2Si), magnesium boride (MgB_2), calcium hexaboride (CaB_6), aluminum oxide (Al_2O_3), and titanium dioxide (TiO_2) ceramics [48], and are depicted in Fig. 10 (a-e) & Fig. 11 (a-e), accordingly. At 0.2 MeV, 0.662 MeV (^{137}Cs), & 1.25 MeV (^{60}Co) photon energies, sample B5 has lower HVL & MFP compared to all five commercial glasses values (see Fig. 10 (a) & Fig. 11 (a)). Besides, glass B5 owns evidently smaller HVL & MFP than compared all five forms of alloys up to 0.6 MeV 'E', except at 15 KeV 'E' (CN & MN400 alloys owns lesser values for 15 KeV 'E' than sample B5) concerning 0.015–15 MeV 'E' range (Fig. 10 (b) & Fig. 11 (b)). Also, within 'E' range of 15 KeV–15 MeV, in contrast to six kinds of polymers, seven types of concretes, and six forms of ceramics quantities, glass B5 possesses fewer HVL & MFP, respectively, except than Pb where Pb has minimal values at all tested energies (see Fig. 10 (c, d & e) & Fig. 11 (c, d, & e)). So, specifically, glass B5 with relatively less thickness is ample to effectively attenuate photons as opposed to distinct commercial glasses, polymers, concretes, and ceramics.
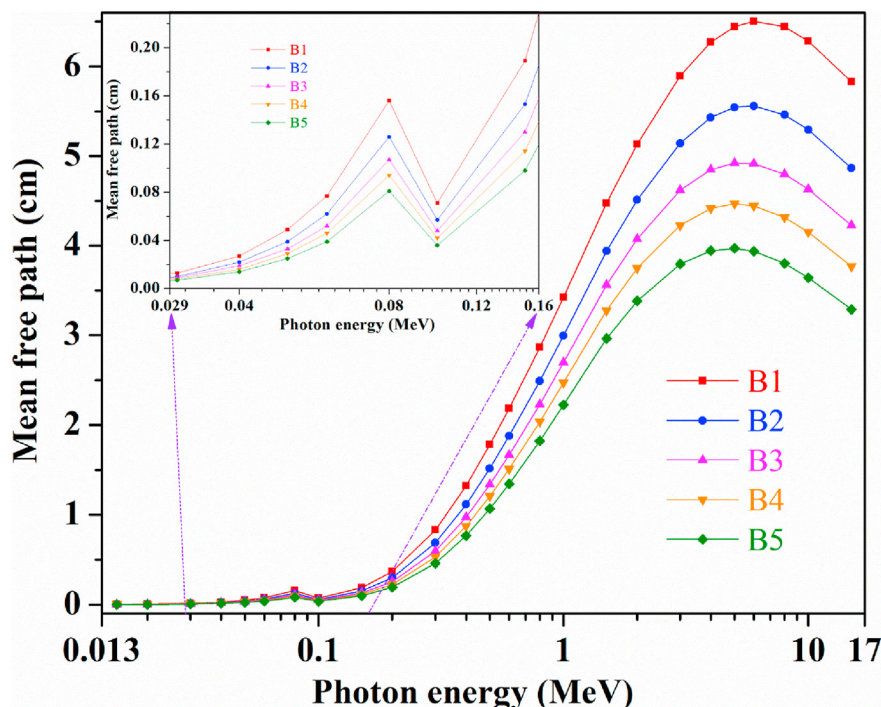

(a)

(b)

Fig. 8 – Variations of (a) half-value layer (HVL) and (b) tenth-value layer (TVL) with photon energy (MeV) (insets, within the 0.029–0.16 MeV photon energy range) for all B1–B5 glasses.

Fig. 9 − Variation of mean free path (MFP) with photon energy (MeV) (inset, within the range of 0.029−0.16 MeV photon energy) for all B1−B5 glasses.

Corresponding Fig. 12 (a-e) & (f-j) present the reckoned EBFs & EABFs variations within inspected 'E' range at 1, 2, 5, 10, 15, 20, 25, 30, 35, and 40 mfp PDs for all B1−B5 glasses. For these five chosen samples, for calculated Z_{eq} & G–P fitting parameters (b, c, a, X_k, and d) data related to EBFs & EABFs computations within 0.015−15 MeV 'E' region readers' can refer to Table S1S5 in Supplementary Material. Following Fig. 12, one can observe three explicit sections of EBFs & EABFs as against 'E' which are principally relevant to PEA, CS, and PP phenomena, individually. Here, for all B1−B5 samples, EBFs & EABFs curves follow an identical movement with both 'E' & PD. Because of PEA, EBFs & EABFs for all B1−B5 glasses are minimal at lower 'E' range (0.015−0.3 MeV) as PEA eliminates photons from the glass, blocking them to buildup. But, at 0.02, 0.06, and 0.1 MeV 'E' i.e., near 'Bi' L1 (=0.0163875 MeV) & K-absorption edges higher buildup of photons has transpired. Further, from B1→B5 sample, as 'Bi' improves from 56.1448 wt % → 74.6161 wt% (see Table 1), at 0.1 MeV 'E' peak, a gradually enhanced photons 'buildup' occurs (see Fig. 12). Later, > 0.3 up to 3 MeV 'E', for all studied glasses, EBFs & EABFs are regularly increased owing to the CS dominance as this mechanism causes to an only fractional reduction in 'E' by scattering and can not pluck out photons wholly, and here longer lifetimes of them make escape chances higher through the glass, resulting in larger EBFs & EABFs. Further, above 3 MeV up to 15 MeV 'E', the PP process is effective in all B1−B5 glasses, and due to this phenomenon EBFs & EABFs are enhanced at high energies and greater PDs (>10 mfp), except at smaller PDs like 1 & 2 mfp. However, the CS can not be ruled out completely and could

occur at all energies and in all substances. At bigger energies, secondary γ-rays are created due to complex scattering actions, leading to photons improved buildup. Also, with PD increment, consequently, thickness enlargement, commonly, in high-Z_{eq} media these scatterings yields hugh γ-ray 'buildups' due to available large scattering volume. Glass B5 (high Bi_2O_3 quantity, 42.5 mol%) by possessing greater Z_{eq}/Z_{eff} has the lower estimated EBFs & EABFs in all selected samples.

Within the tested 'E' range, for all B1−B5 samples (t = 7 mm), the assessed RPE discrepancies are portrayed in Fig. 13. From this plot, one can observe that the Bi_2O_3 content growth from 20 mol% (B1 sample) to 42.5 mol% (B5 glass) as against B_2O_3 improves the photons attenuation feature, because as a high-Z element, Bi, incessantly aids the collisions between photons and glasses as opposed to 'B' (light element). Hence, in all selected glasses, sample B5 reveals analogously greater RPE within the studied 'E' region. The incident photons with 'E' 15−60 KeV can be totally soaked up in all B1, B2, B3, B4, and B5 glasses, even after, up to 0.15 MeV 'E' all these five samples have fairly large RPE, say, for 150 KeV 'E', exclusively, 97.52%, 98.97%, 99.54%, 99.78%, and 99.92%. Afterward, undeniably, for all B1−B5 samples, with advancing 'E', RPE reduced exponentially, proclaiming that the incoming larger energy photons are capable of pass over these glasses with ease. For instance, the RPE for B1 & B2 samples are 10.21% & 11.83%, respectively, for 6 MeV 'E' photons, and for 5 MeV 'E' penetrating γ-rays, for B3, B4, and B5 glasses, 13.26%, 14.51%, and 16.16% are the corresponding RPE. These results insinuate that, for example, glass B5 can absorb or attenuate at most
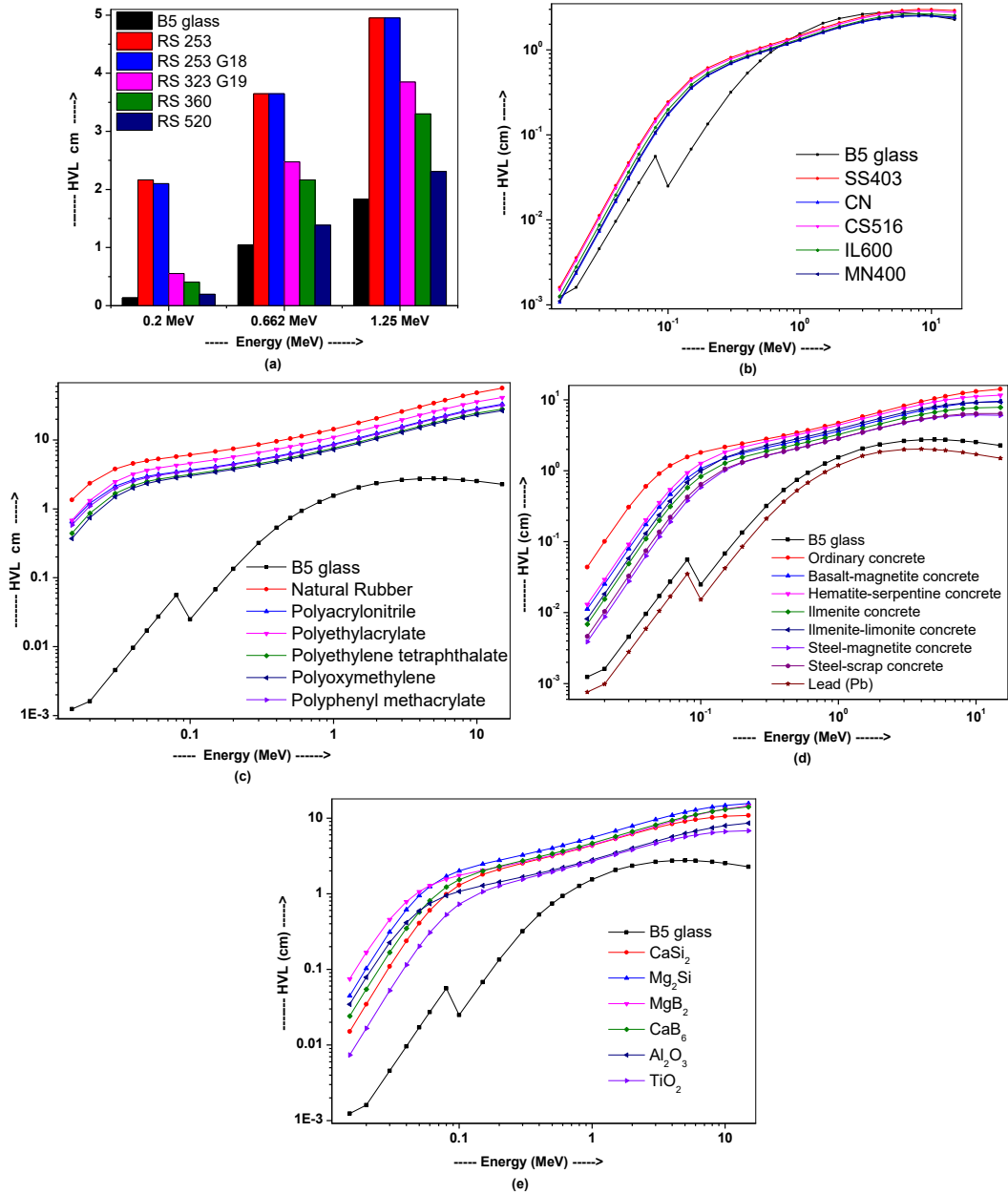
Fig. 10 – Comparison of HVL of the glass 'B5' with some (a) commercial glasses, (b) alloys, (c) polymers, (d) standard shielding concretes and Lead, and (e) Ceramics.

16.16% of the 5 MeV 'E' photons and the rest of 83.84% could go through it. Later, for 15 MeV 'E' photons, from B1→B5 glass, 11.31%, 13.4%, 15.27%,16.95%, and 19.18% are the discrete estimated RPE. From Fig. 13, conspicuously, the obtained RPE issues confirm selected B_2O_3–Bi_2O_3 glasses favorable photon shielding ability for lower energies in contrast to greater ones.

Fig. 14 (a) & (b) represents the corresponding estimated 'Ψ_P' & 'Ψ_A' divergences within the KE range of 15 KeV–15 MeV for all B1–B5 glasses. Here, one can observe that both Ψ_P (protons (charge = +1)) & Ψ_A (α-particles (charge = +2)) patterns for all selected glasses show the same drifts with KE. As KE raises from 0.015 MeV both Ψ_P & Ψ_A are increased primarily. At

90 KeV for sample B1 & 100 KeV for glasses B2, B3, B4, and B5, maximal Ψ_P values are identified while at 0.7 MeV KE the highest Ψ_A quantities are noticed for all B1–B5 samples. Later, both Ψ_P & Ψ_A of all studied glasses are reduced consistently with additional KE increment up to considered 15 MeV. As α-particles possess larger mass (=6.645 × 10^{-24} g), consequently, smaller speed relative to protons (mass = 1.673 × 10−24 g), greater MSPs are perceived for α-particles and also these particles reach the most at bigger KE compared to protons as α-particles lose less KE (electronic excitation & ionization of atoms) by interacting with outer orbital electrons of atoms in glasses. Here, sample B5, which owns the highest 'Bi' element
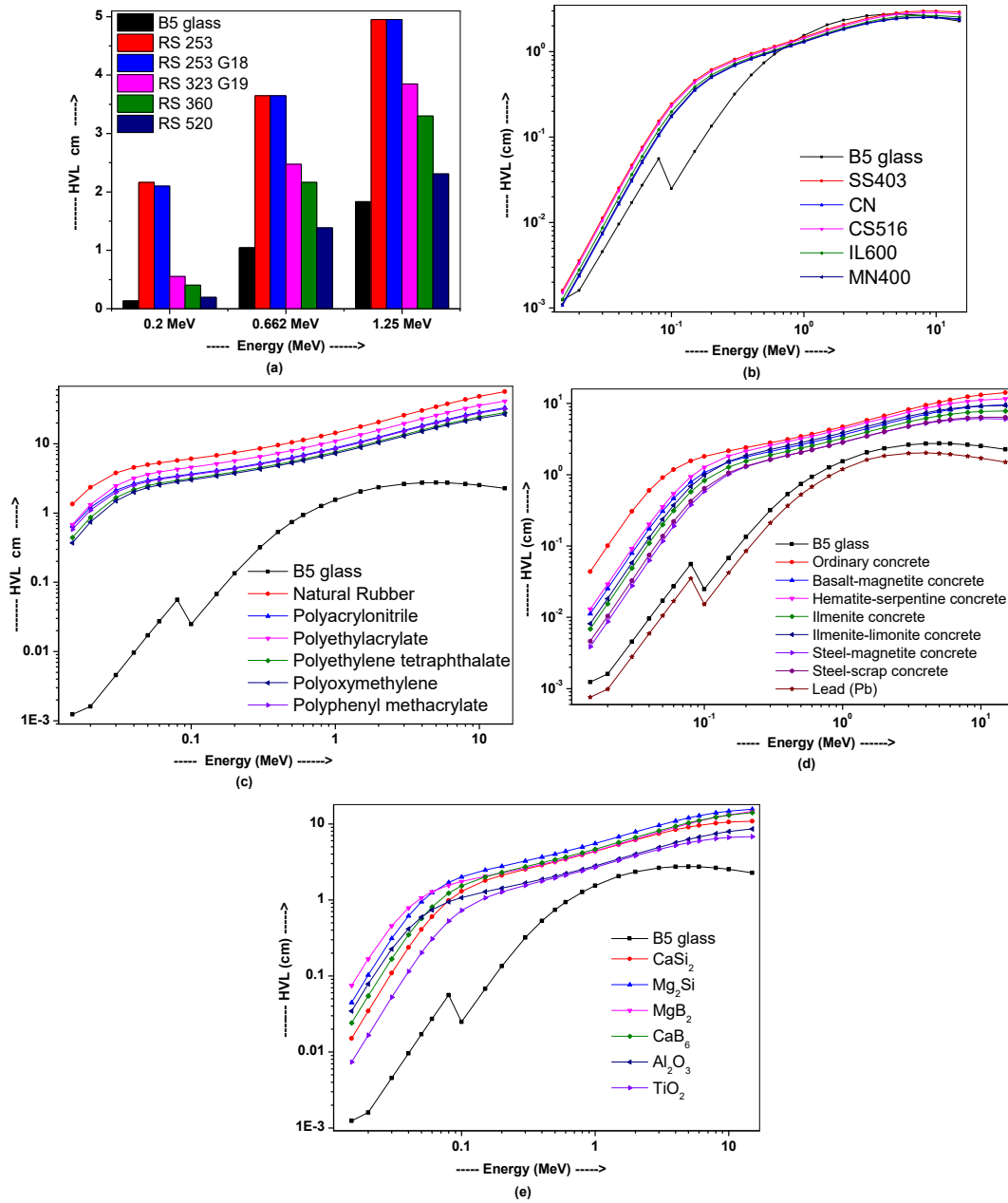
Fig. 11 — Comparison of MFP of the glass 'B5' with some (a) commercial glasses, (b) alloys, (c) polymers, (d) standard shielding concretes and Lead, and (e) Ceramics.

weight, 74.6161 wt%, exhibits relatively lower Ψ_P & Ψ_A in all B1−B5 glasses, i.e., more competent in ceasing bombarding protons and α-particles, which can also be connected to its heavier 'ρ' (high Bi_2O_3 add-on).

Likewise, for all B1−B5 glasses, Fig. 15 (a) & (b) shows calculated Φ_P & Φ_A changes graphically within 0.015−15 MeV KE region, accordingly, and the respective inset plots display the zoom-in KE range at −0.02−2.1 MeV. Generally, for best proton & α-particle freezing potential, lower 'PRs' are imperative for materials. It is apparent from Fig. 15 results that with KE, both the Φ_P & Φ_A gradationally reduced as Bi_2O_3 content increases from sample B1→B5 in reference to B_2O_3

implying that sample B5 possesses the better terminating ability for protons & α-particles. Besides, from 15 KeV up to 15 MeV KE both Φ_P & Φ_A values of all studied glasses have grown nearly linearly. Here, it is identified that the range of α-particles is shorter in contrast to that of protons and basically ~1/9 quantity of Φ_P is reasonable to attenuate the incoming α-particles. At the explored KE range, for glass B5, the computed Φ_P & Φ_A quantities are varied within 0.1381−992.42 μm & 0.0935−112.12 μm ranges, respectively.

Accessorily, within the KE range of 15 KeV–15 MeV, for all B1−B5 samples, corresponding Fig. 16 (a) & (b) illustrates the derived 'Ψ_E' & CSDA range variabilities whereas the
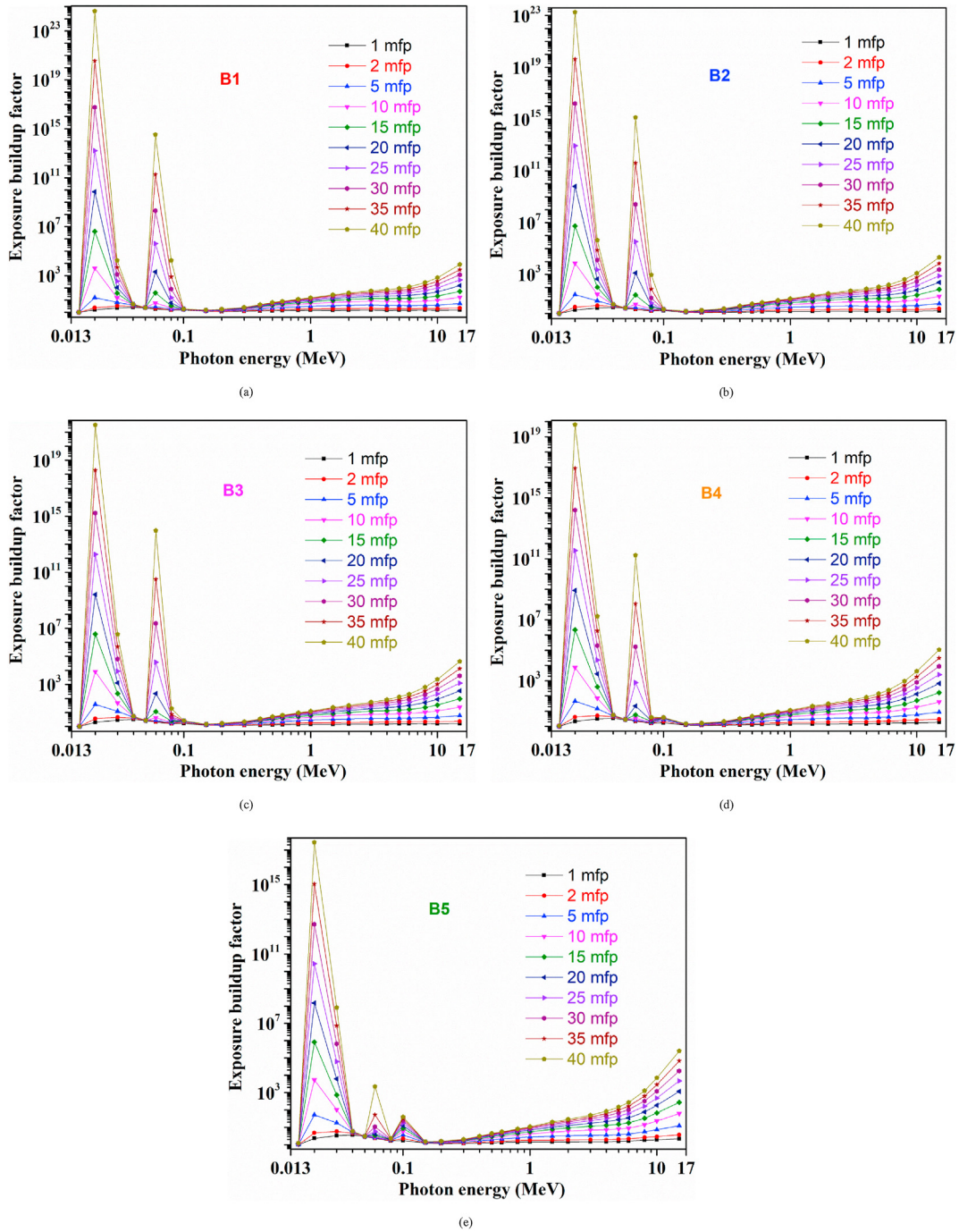
Fig. 12 – Variations of (a–e) exposure buildup factor (EBF) and (f–j) energy absorption buildup factor (EABF) with photon energy at different mean free paths for all B1–B5 glasses.
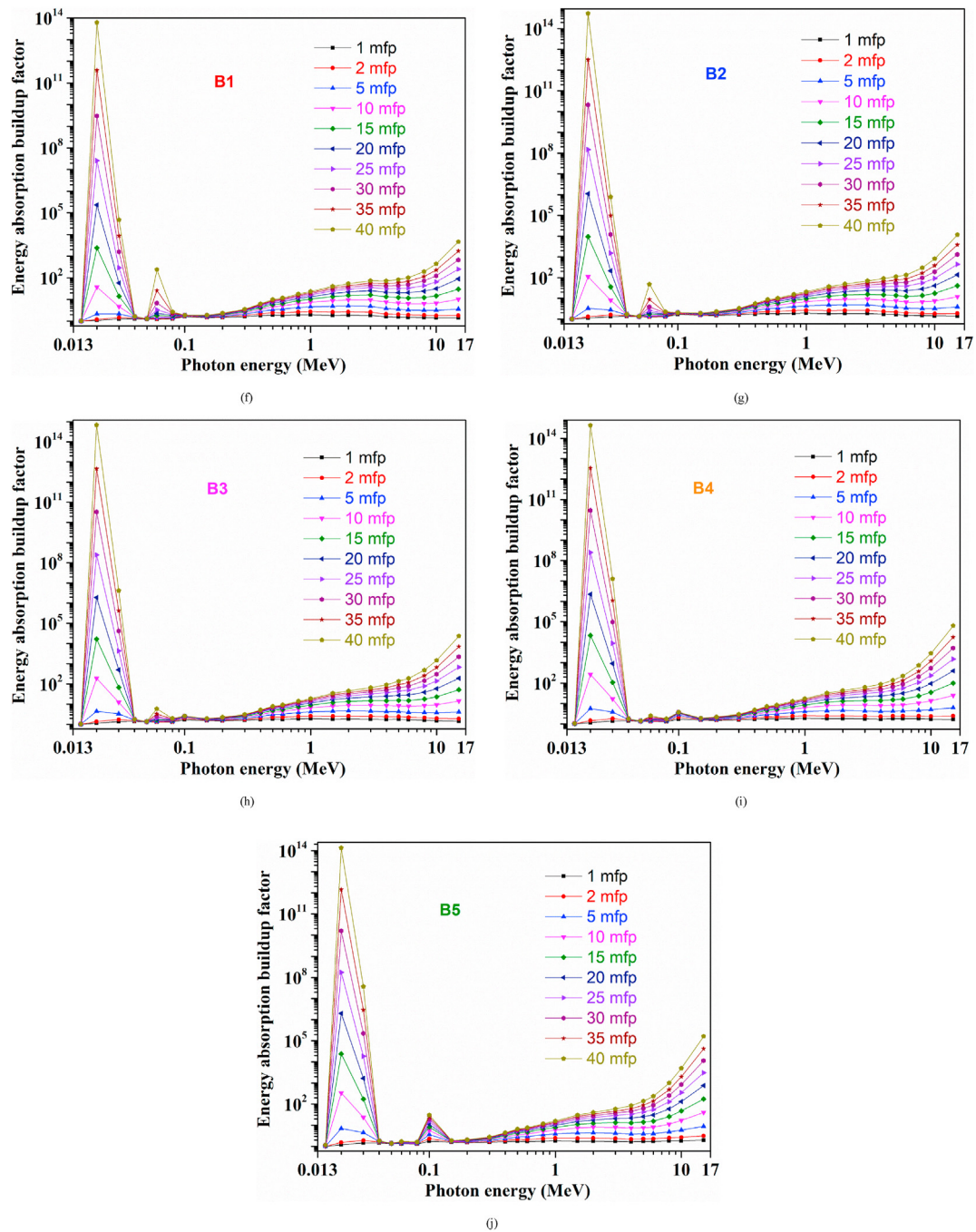
(f)

(g)

(h)

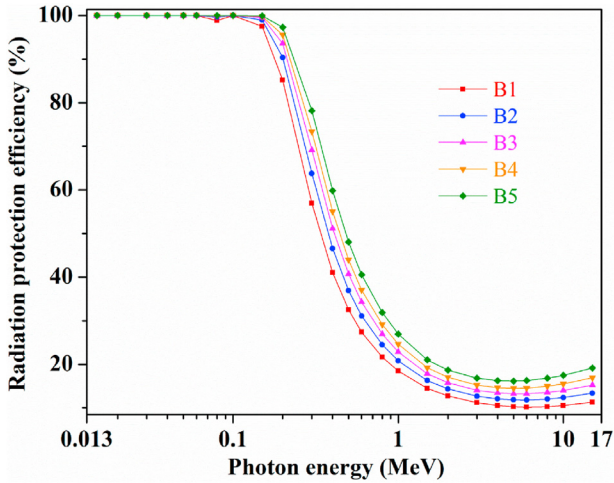
(i)

(j)

Fig. 12 — (*continued*).

Fig. 13 – Variation of radiation protection efficiency (RPE) with photon energy (MeV) for all B1–B5 samples.

respective inset plots exhibit expanded KE ranges at 0.9–15.5 MeV & 0.014–0.21 MeV. Following Fig. 16 (a) one can notice that with the electron KE, 'Ψ_E' decline from sample B1→B5, and has the lowest values at 0.9 MeV for B1–B4 glasses, and 0.8 MeV for sample B5 with enhancing KE. Then, 'Ψ_E' quantities increase nominally up to 15 MeV KE for all B1–B5 glasses.

However, the CSDA ranges increase with electron KE though the 'Ψ_E' reduces (see Fig. 16 (b)). Usually, at lower KE, the electrons very frequently collide with low-Z compounds owing to high N_{eff} (see Fig. 7) while with enhancing KE more interactions of electrons may happen for high-Z substances [27]. Here, B1 glass is influential to shield low KE electrons whereas sample B5 is effective in attenuating greater KE electrons which is on grounds of the Bremsstrahlung radiation.

As a consequence of regulated nuclear fission reactions (heavier nucleus progression into lighter nuclei), commonly, neutrons are created. Banking on KE, neutrons are
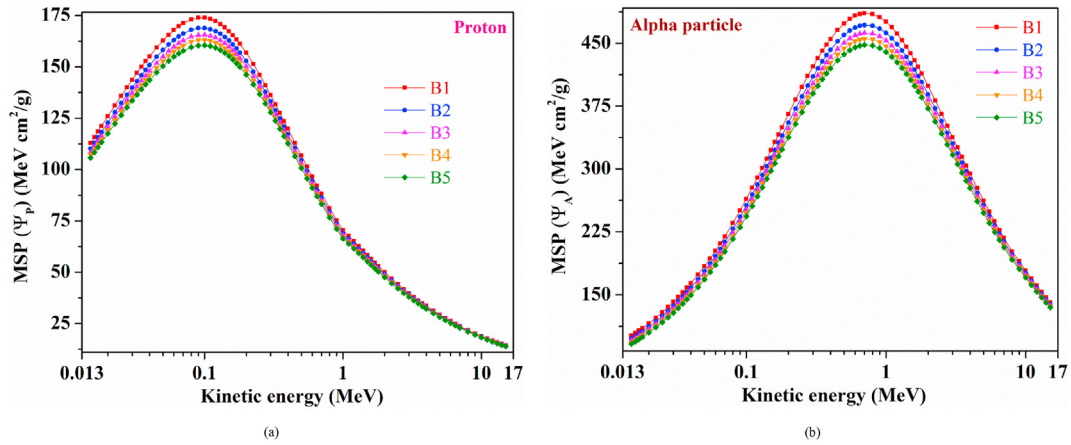

Fig. 14 – Variations of (a) proton mass stopping power (Ψ_P) and (b) alpha mass stopping power (Ψ_A) as a function of kinetic energy (KE) for all B1–B5 glasses.
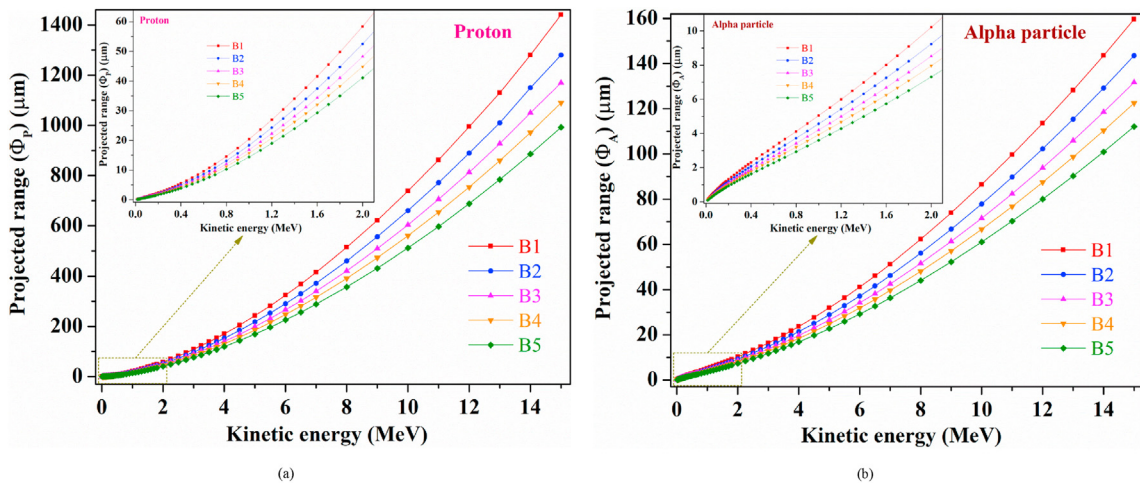

Fig. 15 – Variations of (a) proton projected range (Φ_P) and (b) alpha projected range (Φ_A) as a function of kinetic energy (KE) (insets, within KE regions at −0.02−2.1 MeV) for all B1–B5 glasses.
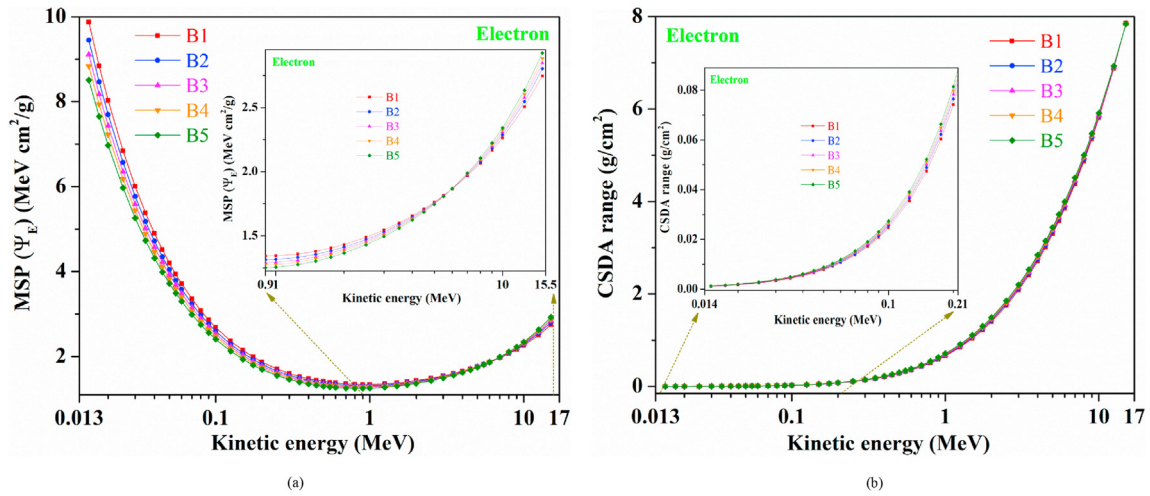
Fig. 16 − Variations of (a) electron stopping power (Ψ_E) (inset, within the range of 0.9−15.5 MeV KE) and (b) CSDA range (inset, within the 0.014−0.21 MeV KE range) as a function of kinetic. energy (KE) for all B1−B5 samples.

Table 3 − Effective removal cross-sections for fast neutrons Σ_R (cm^{-1}) for all B1−B5 glasses.

Glass Code	Element	Σ_R/ρ (cm^2/g)	Fraction by weight %	Partial Density (g/cm^3)	Σ_R (cm^{-1})
B1	B	0.0575	0.116179	0.499802058	0.02873861834
	O	0.0405	0.322373	1.386848646	0.05616737016
	Bi	0.0103	0.561448	2.415349296	0.02487809775
					Σ_R = **0.1097840863**
	Total Σ_R for glass 'B1' = **0.10978** cm^{-1}				
B2	B	0.0575	0.096124	0.468412252	0.02693370449
	O	0.0405	0.284505	1.386392865	0.05614891103
	Bi	0.0103	0.619371	3.018194883	0.03108740729
					Σ_R = **0.1141700228**
	Total Σ_R for glass 'B2' = **0.11417** cm^{-1}				
B3	B	0.0575	0.080285	0.431853015	0.02483154836
	O	0.0405	0.254598	1.369482642	0.055464047
	Bi	0.0103	0.665117	3.577664343	0.03684994273
					Σ_R = **0.1171455381**
	Total Σ_R for glass 'B3' = **0.11714** cm^{-1}				
B4	B	0.0575	0.067459	0.393555806	0.02262945885
	O	0.0405	0.230381	1.344042754	0.05443373154
	Bi	0.0103	0.70216	4.09640144	0.04219293483
					Σ_R = **0.1192561252**
	Total Σ_R for glass 'B4' = **0.11926** cm^{-1}				
B5	B	0.0575	0.052224	0.336374784	0.01934155008
	O	0.0405	0.201615	1.298602215	0.05259338971
	Bi	0.0103	0.746161	4.806023001	0.049950203691
					Σ_R = **0.1214369767**
	Total Σ_R for glass 'B5' = **0.12144** cm^{-1}				

Table 4 − Comparison of Σ_R (cm^{-1}) of glass B5 with reported various nuclear radiation shielding materials.

Sample	Σ_R	Reference
'B5' glass	0.12144	Present work
Graphite (C)	0.0773	[49]
Water (H_2O)	0.1023	
Polyethylene grains	0.0789	
Ethanol (C_2H_6O)	0.0939	
B_4C	0.0714	
Ordinary concrete (OC)	0.0937	[47]
Hematite-serpentine concrete (HSC)	0.0967	
Ilmenite-limonite concrete (ILC)	0.0950	
Basalt-magnetite concrete (BMC)	0.1102	
Ilmenite concrete (IC)	0.1121	
Steel-scrap concrete (SSC)	0.1247	
Steel-magnetite concrete (SMC)	0.1420	
TZN-D glass	0.108	[25]
SCNZ5 glass	0.053077264	[26]
H5 glass	0.138	[27]
TBBT30 glass	0.116862332	[28]
L15 glass	0.104	[29]
Fe-05 composite	0.0924	[50]
Pd50Mn50 alloy	0.161	[51]
Polyethersulfone (PES) polymer	0.088	[52]

categorized as thermal (0.0253 eV KE) or slow neutrons (<0.5 eV KE), epithermal or medium neutrons (up to 5 KeV KE), and fast neutrons (>500 KeV KE) [5]. Table 3 presents the 'Σ_R' calculation steps and the correlated Σ_R quantities for all B1−B5 glasses. 0.10978 cm^{-1}, 0.11417 cm^{-1}, 0.11714 cm^{-1}, 0.11926 cm^{-1}, and 0.12144 cm^{-1}, respectively, are the obtained Σ_R for B1, B2, B3, B4, and B5 samples. Here, glass B5 (B: 5.2224 wt%, Bi: 74.6161 wt%, O: 20.1615 wt%) possesses the largest Σ_R in all selected glasses, signifying that it has correspondingly greater efficacy to shield fast neutrons. This

means, though ^{10}B atom owns a large neutron absorption cross-section (σ_A = 760 b, 1 b = 10^{-28} m^2), heavy element 'Bi' also takes part in boosting Σ_R (see Table 3) as for any certain medium, high 'ρ' (e.g., sample B5, ρ = 6.441 g/cm^3) is desirable in fast neutrons shielding, requiring both lighter & heavier elements appropriate mixtures in it. Glass B1 holds the minimum Σ_R relying on the according B, Bi, and O elements whole participations in it.

Supplementarily, glass B5 'Σ_R' is correlated with corresponding alternative classical neutron shields and some other just recently reported distinct radiation shielding materials Σ_R [25−29, 47, 49, 50−52] and the related outcomes are presented in Table 4. Here, sample B5 has greater Σ_R than C, H_2O, Polyethylene grains, C_2H_6O, & B_4C [49], OC, HSC, ILC, BMC, & IC [47], and TZN-D [25], SCNZ5 [26], TBBT30 [28], & L15 [29] glasses, Fe-

05 composite [50], and PES polymer [52], and a lower quantity in contrast to SSC & SMC [47], H5 glass [27], and Pd50Mn50 alloy [51] Σ_R. In our previous work, for GeO_2-Tl_2O–Bi_2O_3 glass system, appropriate γ & neutron shielding aspects were reported [53].

4. Conclusions

In the current study, directly and indirectly ionizing radiations (γ, proton, α-, e^-, & neutron) attenuation competences for chosen five bismuth borate glasses were explored by scrutinizing all appropriate μ, μ/ρ, Z_{eff}, N_{eff}, HVL, TVL, MFP, Z_{eq}, EBF, EABF, RPE, Ψ_P, Φ_P, Ψ_A, Φ_A, Ψ_E, CSDA ranges, and Σ_R variables. Theoretically (by Phy-X/PSD) deduced μ/ρ quantities were validated with computationally (utilizing respective MCNPX, Geant4, and FLUKA codes) obtained μ/ρ outputs for all B1–B5 glasses. For instance, at 15 KeV energy, 65.3893, 72.1961, 77.1494, 81.7293, and 86.298 cm^2/g were μ/ρ (using FLUKA code), correspondingly, for B1, B2, B3, B4, and B5 samples while for the same glasses at the same energy, 65.753, 72.391, 77.633, 81.878, and 86.92 cm^2/g were the respective calculated μ/ρ values applying Phy-X/PSD. Bi_2O_3 insertion in place of B_2O_3 demonstrated an advantageous impact on γ-ray shielding abilities (enhanced Z_{eff} and a reduction in HVL, TVL, & MFP) in all B1–B5 glasses, at any selected photon energy. For example, at 15 MeV energy, for glass B5, which owns the lowest HVL, TVL, & MFP in all B1–B5 samples, 2.279 cm, 7.569 cm, and 3.287 cm were the derived according values. Also, proportionately, sample B5 has smaller HVL & MFP than corresponding quantities of five commercial glasses at 0.2, 0.662, and 1.25 MeV γ-ray energies, and six types of polymers, seven kinds of concretes & six forms of ceramics within photon energy range of 0.015–15 MeV. Moreover, at 1–40 mfp with selected 10 PDs, for assessed EBFs & EABFs, for all B1–B5 glasses within 15 KeV–15 MeV photon energy range, at lower, medium, and larger energy ranges individual PEA, CS, and PP mechanisms supremacy was recognized. Additionally, for all selected samples, Ψ_P, Φ_P, Ψ_A, Φ_A, Ψ_E, and CSDA range for electrons values within 0.015–15 MeV KE range were estimated. Further, in all B1–B5 glasses, the B5 sample (Bi: 74.6161 wt% & B: 5.2224 wt%) exhibits relatively higher Σ_R (=0.12144 cm^{-1}) as Bi_2O_3 improves the glasses 'ρ' (4.302 g/cm^3 →6.441 g/cm^3). Comprehensively, larger 'ρ' (=6.441 g/cm^3), bigger μ, μ/ρ, Z_{eff}, Z_{eq}, RPE, & minimal HVL, TVL, MFP, EBFs, EABFs, fewer ranges for protons, α-, and e^-, greater Σ_R of glass B5 among all inspected glasses revealed its better shielding capacity for all γ, proton, α-, and e^- radiations, and fast neutrons. Thus, glass B5 can be utilized as a nuclear waste storage container and as a potential radiation shielding medium at nuclear reactors and nuclear medicine facilities.

CRediT author statement

G. Lakshminarayana: Conceptualization, Visualization, Writing - Original Draft, Writing - Review and Editing, Supervision **Ashok Kumar**: Software, Formal analysis, Data Curation, Validation **H.O. Tekin**: Software, Formal analysis, Data Curation **Shams A.M. Issa**: Software, Formal analysis, Data Curation **M.S. Al-Buriahi**: Software, Formal analysis, Data Curation **Dong-Eun Lee**: Project administration, Funding acquisition, Supervision **Jonghun Yoon**: Supervision **Taejoon Park**: Project administration, Funding acquisition, Supervision.

Declaration of Competing Interest

The authors declare that they have no known competing financial interests or personal relationships that could have appeared to influence the work reported in this paper.

Acknowledgements

Appendix A. Supplementary data

Supplementary data to this article can be found online at https://doi.org/10.1016/j.jmrt.2020.10.019.

REFERENCES

[1] https://www.iaea.org/newscenter/news/preliminary-nuclear-power-facts-and-figures-for-2019.

[2] Mettler Jr FA, Guiberteau MJ. Essentials of nuclear medicine imaging. 6th ed. Philadelphia, PA: Saunders Elsevier; 2012. p. 607. Hardcover ISBN: 978-1455701049.

[3] Osmanlioglu AE. Investigation of shielding material in radioactive waste management − 13009. In: WM2013 conf. Arizona, USA: Phoenix; 2013.

[4] DeVanzo M, Hayes RB. Ionizing radiation shielding properties of metal oxide impregnated conformal coatings. Radiat Phys Chem 2020;171:108685.

[5] Kaplan MF. Concrete radiation shielding: nuclear Physics, concrete properties, design and construction. Harlow, Essex, England: Longman scientific and Technology, Longman Group UK Limited; 1989.

[6] Mirhosseini SS. "The Effects of nuclear Radiation on aging reinforced concrete Structures in nuclear power plants". Master's thesis. Canada: University of Waterloo; 2010. UWSpace, http://hdl.handle.net/10012/5452.

[7] Reda AM, El-Daly AA. Gamma ray shielding characteristics of Sn-20Bi and Sn-20Bi-0.4Cu lead-free alloys. Prog Nucl Energy 2020;123:103304.

[8] Issa SAM, Rashad M, Hanafy TA, Saddeek YB. Experimental investigations on elastic and radiation shielding parameters of WO_3-B_2O_3-TeO_2 glasses. J Non-Cryst Solids 2020;544:120207.

[9] Alatawi A, Alsharari AM, Issa SAM, Rashad M, Darwish AAA, Saddeek YB, et al. Improvement of mechanical properties and radiation shielding performance of $AlBiBO_3$ glasses using yttria: an experimental investigation. Ceram Int 2020;46:3534−42.

[10] Lakshminarayana G, Dong MG, Al-Buriahi MS, Kumar A, Lee D-E, Yoon J, et al. B_2O_3–Bi_2O_3–TeO_2–BaO and TeO_2–Bi_2O_3–BaO glass systems: a comparative assessment of gamma-ray and fast and thermal neutron attenuation aspects. Appl Phys A 2020;126:1–18.

[11] Siengsanoh K, Hongtong W, Chaiphaksa W, Limkitjaroenporn P, Kaewkhao J. Physical, optical and gamma-ray shielding properties of BaO-La_2O_3-B_2O_3 and BaO-Na_2O-B_2O_3 glass systems at 662 keV. J Phys: Conf. Series 2019;1259:1–8.

[12] Plodinec MJ. Borosilicate glasses for nuclear waste imobilisation. Glass Technol 2000;41:186–92.

[13] Lee AC, Lee SK. Network polymerization and cation coordination environments in boron-bearing rhyolitic melts: insights from ^{17}O, ^{11}B, and ^{27}Al solid-state NMR of sodium aluminoborosilicate glasses with varying boron content. Geochem Cosmochim Acta 2020;268:325–47.

[14] Lakshminarayana G, Baki SO, Lira A, Kityk IV, Mahdi MA. Structural, thermal, and optical absorption studies of Er3 +, Tm3 +, and Pr3 +-doped borotellurite glasses. J Non-Cryst Solids 2017;459:150–9.

[15] Saritha D, Markandeya Y, Salagram M, Vithal M, Singh AK, Bhikshamaiah G. Effect of Bi_2O_3 on physical, optical and structural studies of ZnO–Bi_2O_3–B_2O_3 glasses. J Non-Cryst Solids 2008;354:5573–9.

[16] Tiefeng X, Feifei C, Shixun D, Qiuhua N, Xiang S, Xunsi W. Third-order optical nonlinear characterizations of Bi_2O_3–B_2O_3–TiO_2 ternary glasses. Phys Biol 2009;404:2012–5.

[17] Lakshminarayana G, Kebaili I, Dong MG, Al-Buriahi MS, Dahshan A, Kityk IV, et al. Estimation of gamma-rays, and fast and the thermal neutrons attenuation characteristics for bismuth tellurite and bismuth boro-tellurite glass systems. J Mater Sci 2020;55:5750–71.

[18] Lakshminarayana G, Elmahroug Y, Kumar A, Dong MG, Lee D-E, Yoon J, et al. TeO_2–B_2O_3–ZnO–La_2O_3 glasses: γ-ray and neutron attenuation characteristics analysis by WinXCOM program, MCNP5, Geant4, and Penelope simulation codes. Ceram Int 2020;46:16620–35.

[19] Tekin HO, Issa SAM, Kavaz E, Guclu EEA. The direct effect of Er_2O_3 on bismuth barium telluro borate glasses for nuclear security applications. Mater Res Express 2019;6:115212.

[20] Rammah YS, Mahmoud KA, Kavaz E, Kumar A, El-Agawany FI. The role of PbO/Bi_2O_3 insertion on the shielding characteristics of novel borate glasses. Ceram Int 2020;46(15):23357–68. https://doi.org/10.1016/j.ceramint.2020.04.018.

[21] Kurtulus R, Kavas T. Investigation on the physical properties, shielding parameters, glass formation ability, and cost analysis for waste soda-lime-silica (SLS) glass containing SrO, Radiat. Phys Chem 2020;176:109090.

[22] Olarinoye IO, El-Agawany FI, El-Adawy A, Yousef El S, Rammah YS. Mechanical features, alpha particles, photon, proton, and neutron interaction parameters of TeO_2–V_2O_3–MoO_3 semiconductor glasses. CeramInt 2020;46(14):23134–44. https://doi.org/10.1016/j.ceramint.2020.06.093.

[23] Kavaz E, Tekin HO, Kilic G, Susoy G. Newly developed Zinc-Tellurite glass system: an experimental investigation on impact of Ta_2O_5 on nuclear radiation shielding ability. J Non-Cryst Solids 2020;544:120169.

[24] Abouhaswa AS, Kavaz E. A novel B_2O_3-Na_2O-BaO-HgO glass system: synthesis, physical, optical and nuclear shielding features. Ceram Int 2020;46:16166–77.

[25] Al-Buriahi MS, Bakhsh EM, Tonguc B, Khan SB. Mechanical and radiation shielding properties of tellurite glasses doped with ZnO and NiO. Ceram Int 2020;46:19078–83.

[26] Akyildirim H, Kavaz E, El-Agawany FI, Yousef E, Rammah YS. Radiation shielding features of zirconolite silicate glasses using XCOM and FLUKA simulation code. J Non-Cryst Solids 2020;545:120245.

[27] Kaur P, Singh KJ, Thakur S, Kurudirek M. Investigation of a competent non-toxic Bi_2O_3–Li_2O–CeO_2–MoO_3–B_2O_3 glass system for nuclear radiation security applications. J Non-Cryst Solids 2020;545:120235.

[28] Rammah YS, Kavaz E, Akyildirim H, El-Agawany FI. Evaluation of photon, neutron, and charged particle shielding competences of TeO_2-B_2O_3-Bi_2O_3-TiO_2 glasses. J Non-Cryst Solids 2020;535:119960.

[29] Kaur P, Singh KJ, Thakur S. Gamma-ray, neutron and beta radiation shielding properties of Bi_2O_3-Li_2O-MnO_2-B_2O_3 glasses. J Phys: Conf. Series 2020;1531:012043.

[30] Becker P. Thermal and optical properties of glasses of the system Bi_2O_3 − B_2O_3. Cryst Res Technol 2003;38:74–82.

[31] Lakshminarayana G, Dong MG, Kumar A, Elmahroug Y, Wagh A, Lee D-E, et al. Assessment of gamma-rays and fast neutron beam attenuation features of Er_2O_3-doped B_2O_3–ZnO–Bi_2O_3 glasses using XCOM and simulation codes (MCNP5 and Geant4). Appl Phys A 2019;125:1–14.

[32] Iqbal A, Ullah N, Ur Rahman A. Density-dependent energy loss of protons in Pb and Be targets and percent mass-stopping power from bethe-bloch formula and bichsel-sternheimer data within 1–12 MeV energy range: a comparative study based on bland-altman analysis. J Med Imag Radiat Sci 2019;50:149–56.

[33] Seltzer SM, Berger MJ. Procedure for calculating the radiation stopping power for electrons. Int J Appl Radiat Isot 1982;33:1219–26.

[34] Ziegler JF, Ziegler MD, Biersack JP. Srim − the stopping and range of ions in matter. Nucl Instrum Methods Phys Res, Sect B 2010;268:1818–23.

[35] Berger MJ, Coursey JS, Zucker MA, Chang J, Estar PSTAR, ASTAR. Stopping-power & range Tables for electrons, protons, and helium Ions. Updated 2017. NIST; 2017. https://doi.org/10.18434/T4NC7P. https://www.nist.gov/pml/stopping-power-range-tables-electrons-protons-and-helium-ions.

[36] Şakar E, Özpolat ÖF, Alım B, Sayyed MI, Kurudirek M. Phy-X/PSD: development of a user friendly online software for calculation of parameters relevant to radiation shielding and dosimetry. Radiat Phys Chem 2020;166:108496.

[37] RSICC Computer Code Collection. MCNPX user's manual version 2.4.0. Monte Carlo N-particle transport code system for multiple and high energy applications. 2002.

[38] Agostinelli S, Allison J, Amako K, Apostolakis J, Araujo H, Arce P, et al. GEANT4–A simulation toolkit. Nucl Instrum Methods Phys Res Sect A Accel Spectrom Detect Assoc Equip 2003;506:250–303.

[39] Allison J, Amako K, Apostolakis J, Araujo H, Arce Dubois P, Asai M, et al. Geant4 developments and applications. IEEE Trans Nucl Sci 2006;53:270–278.

[40] Allison J, Amako K, Apostolakis J, Arce P, Asai M, Aso T, et al. Recent developments in Geant4. Nucl Instrum Methods Phys Res Sect A Accel Spectrom Detect Assoc Equip 2016;835:186–225.

[41] Tekin HO. MCNP-X Monte Carlo code application for mass attenuation coefficients of concrete at different energies by modeling 3 × 3 inch NaI(Tl) detector and comparison with XCOM and Monte Carlo Data. Sci Technol Nucl Ins 2016;(2016). https://doi.org/10.1155/2016/6547318. Article ID 6547318/1–7.

[42] Ballarini F, Battistoni G, Brugger M, Campanella M, Carboni M, Cerutti F, et al. The physics of the FLUKA code: recent developments. Adv Space Res 2007;40:1339–1349.

[43] Battistoni G, Boehlen T, Cerutti F, Chin PW, Esposito LS, Fassò A, et al. Overview of the FLUKA code. Ann Nucl Energy 2015;82:10–18.

[44] https://www.schott.com/d/advanced_optics/352fbb5f-4d56-49d3-bb47-256437d58f0a/1.4/schott-radiation-shielding-glass-may-2013-eng.pdf. (Accessed July 2020).

[45] Singh VP, Badiger NM. Gamma ray and neutron shielding properties of some alloy materials. Ann Nucl Energy 2014;64:301–10.

[46] Bhosale RR, More CV, Gaikwad DK, Pawar PP, Rode MN. Radiation shielding and gamma ray attenuation properties of some polymers. Nucl Technol Radiat Protect 2017;32:288–293.

[47] Bashter II. Calculation of radiation attenuation coefficients for shielding concretes. Ann Nucl Energy 1997;24:1389–1401.

[48] Akman F, Khattari ZY, Kaçal MR, Sayyed MI, Afaneh F. The radiation shielding features for some silicide, boride and oxide types ceramics. Radiat Phys Chem 2019;160:9–14.

[49] El Abd A, Mesbah G, Mohammed NMA, Ellithi A. A simple method for determining the effective removal cross section for fast neutrons. J. Rad. Nucl. Appl. 2016;2(2):53–8.

[50] Tekin HO, Akman F, Issa SAM, Kaçal MR, Kilicoglu O, Polat H. Two-step investigation on fabrication and characterization of iron-reinforced novel composite materials for nuclear-radiation shielding applications. J Phys Chem Solid 2020;146:109604.

[51] Tekin HO, Kilicoglu O. The influence of gallium (Ga) additive on nuclear radiation shielding effectiveness of Pd/Mn binary alloys. J Alloys Compd 2020;815:152484.

[52] Thakur S, Kaur P. Comparative analysis of neutron, proton, alpha and beta radiation shielding parameters of PES and PVDC. J Phys: Conf. Series 2020;1531:012003.

[53] Lakshminarayana G, Elmahroug Y, Kumar A, Rekik N, Lee D-E, Yoon J, et al. Reckoning of nuclear radiation attenuation capabilities for binary GeO_2-Tl_2O, GeO_2-Bi_2O_3, and ternary GeO_2-Tl_2O–Bi_2O_3 glasses utilizing pertinent theoretical and computational approaches. Opt Mater 2020;108:110113.